





CRISPR-delivery particles targeting nuclear receptor–interacting protein 1 (*Nrip1*) in adipose cells to enhance energy expenditure

Received for publication, June 22, 2018, and in revised form, August 22, 2018. Published, Papers in Press, September 6, 2018, DOI 10.1074/jbc.RA118.004554

Yuefei Shen[‡], Jessica L. Cohen[‡], Sarah M. Nicoloso[‡], Mark Kelly[‡], Batuhan Yenilmez[‡],  Felipe Henriques[‡],  Emmanouela Tsagkaraki^{‡§}, Yvonne J. K. Edwards[‡], Xiaodi Hu[¶], Randall H. Friedline[¶], Jason K. Kim^{¶¶}, and Michael P. Czech^{‡¶1}

From the [‡]Program in Molecular Medicine and the [¶]Division of Endocrinology, Metabolism, and Diabetes, Department of Medicine, University of Massachusetts Medical School, Worcester, Massachusetts 01605 and the [§]Molecular Basis of Human Disease Graduate Program, School of Sciences, Faculty of Medicine, University of Crete, P.O. Box 2208, Heraklion, Crete 71003, Greece

Edited by Jeffrey E. Pessin

RNA-guided, engineered nucleases derived from the prokaryotic adaptive immune system CRISPR-Cas represent a powerful platform for gene deletion and editing. When used as a therapeutic approach, direct delivery of Cas9 protein and single-guide RNA (sgRNA) could circumvent the safety issues associated with plasmid delivery and therefore represents an attractive tool for precision genome engineering. Gene deletion or editing in adipose tissue to enhance its energy expenditure, fatty acid oxidation, and secretion of bioactive factors through a “browning” process presents a potential therapeutic strategy to alleviate metabolic disease. Here, we developed “CRISPR-delivery particles,” denoted CriPs, composed of nano-size complexes of Cas9 protein and sgRNA that are coated with an amphipathic peptide called Endo-Porter that mediates entry into cells. Efficient CRISPR-Cas9-mediated gene deletion of ectopically expressed GFP by CriPs was achieved in multiple cell types, including a macrophage cell line, primary macrophages, and primary pre-adipocytes. Significant GFP loss was also observed in peritoneal exudate cells with minimum systemic toxicity in GFP-expressing mice following intraperitoneal injection of CriPs containing *Gfp*-targeting sgRNA. Furthermore, disruption of a nuclear co-repressor of catabolism, the *Nrip1* gene, in white adipocytes by CriPs enhanced adipocyte browning with a marked increase of uncoupling protein 1 (UCP1) expression. Of note, the CriP-mediated *Nrip1* deletion did not produce detectable off-target effects. We conclude that CriPs offer an effective Cas9 and sgRNA delivery system for ablating targeted gene products in cultured cells and *in vivo*, providing a potential therapeutic strategy for metabolic disease.

Gene editing based on the CRISPR-associated protein 9 (Cas9) system presents significant therapeutic potential for treating a wide range of diseases (1–4). The CRISPR-Cas9 system, containing the RNA-guided nuclease (Cas9 protein) and a single-guide RNA (sgRNA),² recognizes a protospacer-adjacent motif (PAM) and generates dsDNA breaks at 3 bp upstream of a PAM site (5). dsDNA breaks are repaired by nonhomologous end joining to generate permanent gene deletion by inducing random insertions and deletions (indels) and by homology-directed repair to correct gene mutations with the use of a guide template DNA (5). A key challenge for CRISPR-Cas9-based therapeutics is the efficient, safe delivery of genome editing macromolecules to achieve eventual translation to clinical efficacy and safety (6–9). Viral vectors, including adeno-associated virus (AAV), have shown efficient *in vivo* delivery and expression of CRISPR-Cas9 (10–13). However, it is difficult to fit coding sequences for *Streptococcus pyogenes* Cas9 (SpCas9) plus sgRNAs into AAV vectors due to the restricted packaging capacity of AAVs (14). AAV-based Cas9 delivery also tends to cause significant off-target genome damage due to the sustained expression of Cas9 (15, 16). In addition, the immune response to AAV capsids and the immunogenicity of the long-term existing bacterial Cas9 protein can limit their applications in humans (11). Physical delivery approaches of CRISPR-Cas9, such as electroporation (17–19), microinjection (20), and hydrodynamic injection (21, 22), have also been successfully used, but with concerns such as cell viability, toxicity, and difficulty to apply *in vivo*.

The limitations associated with both viral delivery and physical delivery can be addressed using nonviral delivery systems, such as lipid nanoparticles (23–27), DNA nanoclew (28), and gold nanoparticles (29, 30), as well as chemically conjugating Cas9 protein with polymers (31) and cell-penetrating peptides

These studies were supported by National Institutes of Health Grants DK103047 and DK030898 and a grant from the International Research Alliance of the Novo Nordisk Foundation Center for Metabolic Research (to M. P. C.). The National MMPC at the University of Massachusetts is supported by National Institutes of Health Grant 5U2C-DK093000 (to J. K. K. and M. P. C.). The authors declare that they have no conflicts of interest with the contents of this article. The content is solely the responsibility of the authors and does not necessarily represent the official views of the National Institutes of Health.

This article was selected as one of our Editors' Picks.

This article contains Figs. S1–S3 and Tables S1–S4.

¹ To whom correspondence should be addressed: University of Massachusetts Medical School, 373 Plantation St., Worcester, MA 01605. Tel.: 508-856-2254; Fax: 508-856-1617; E-mail: michael.czech@umassmed.edu.

² The abbreviations used are: sgRNA, single-guide RNA; i.p., intraperitoneal; PAM, protospacer-adjacent motif; indels, insertions and deletions; AAV, adeno-associated virus; RNP, ribonucleoprotein; WAT, white adipose tissue; BAT, brown adipose tissue; CriP, CRISPR-delivery particle; EP, Endo-Porter; GeRP, β -1,3-D-glucan-encapsulated siRNA particle; DLS, dynamic light scattering; 7-AAD, 7-amino-actinomycin D; T7E1, T7 endonuclease I; SNP, single polymorphism; IL, interleukin; IFN, interferon; TNF, tumor necrosis factor; PEC, peritoneal exudate cell; LPS, lipopolysaccharide; DMEM, Dulbecco's modified Eagle's medium; FBS, fetal bovine serum.

Cas9–sgRNA delivery particles for gene deletion

(32). Furthermore, direct delivery of Cas9–sgRNA ribonucleo-protein (RNP) is being considered as a promising therapeutic strategy. Cas9–sgRNA RNP delivery could circumvent the safety problems associated with plasmid delivery, such as uncontrolled integration of DNA segments into the host genome and unwanted immune response to plasmids encoding Cas9 protein and sgRNA (6). Therefore, nonviral delivery of Cas9–sgRNA RNP represents an attractive tool for genome engineering. Cas9–sgRNA RNP delivered by nonviral delivery systems has been tested in cell culture (30, 33), primary cells (15, 19) and for local delivery such as inner ear injection (4, 23), skin injection (18), intratumor injection (28, 34), intramuscular injection (29), and intracranial injection (35). Systemic administration of Cas9 mRNA and sgRNA loaded into a lipid nanoparticle has been reported to achieve robust and persistent genome editing *in vivo* (24), but Cas9–sgRNA RNPs have not been used systemically *in vivo* using a fully nonviral delivery system.

Application of CRISPR in therapies for type 2 diabetes would be attractive because this malady and its complications afflicts around 30 million adults in the United States and is a leading cause of death (36). White adipose tissue (WAT) stores triglycerides and expands greatly during the onset of obesity, which can prompt insulin resistance, failure of insulin secretion, and the development of type 2 diabetes (37). Unlike WAT, brown adipose tissue (BAT) is composed of brown adipocytes that display a high capacity for fat oxidation and a high number of mitochondria containing uncoupling protein 1 (UCP1) for nonshivering thermogenesis that plays a beneficial role in metabolism (38). BAT can also secrete beneficial factors to increase glucose uptake and fatty acid oxidation in other tissues (39, 40). Recent data indicate that increased BAT can favorably control whole-body glucose homeostasis and is associated with lean, insulin-sensitive phenotypes (41–43). White adipocytes can be converted to brown or “beige” adipocytes by silencing molecular targets that suppress energy expenditure, fatty acid oxidation, and insulin signaling, such as the nuclear co-repressor *Nrip1* gene (44, 45) (also denoted as RIP140). *Nrip1* silencing by RNAi in white adipocytes leads to adipocyte “browning” and enhances fatty acid oxidation, mitochondrial respiration, and insulin-mediated glucose uptake (44). *Nrip1* null mice present lean phenotypes with improved insulin sensitivity and glucose tolerance (46), suggesting that *Nrip1* may be a powerful molecular target for alleviating type 2 diabetes and obesity. Here, we developed a novel CRISPR delivery system, denoted CRISPR-delivery particles (CriPs), composed of nano-size complexes of the CRISPR components Cas9 protein and sgRNA targeting a gene of interest, complexed with an Endo-Porter (EP) peptide through electrostatic complexation. EP is an amphipathic α -helical peptide composed of leucine and histidine residues. It is hypothesized that the weak-base histidine residues of EP facilitate the endosomal escape of the cargoes by permeabilizing the endosomal membrane upon acidification within the endosome, known as the “proton-sponge effect” (47). We have previously shown that EP is a crucial component of the β -1,3-D-glucan-encapsulated siRNA particles (GeRPs) and is required for efficient GeRP-mediated siRNA delivery (48–51). As proof of concept, efficient CRISPR-Cas9–

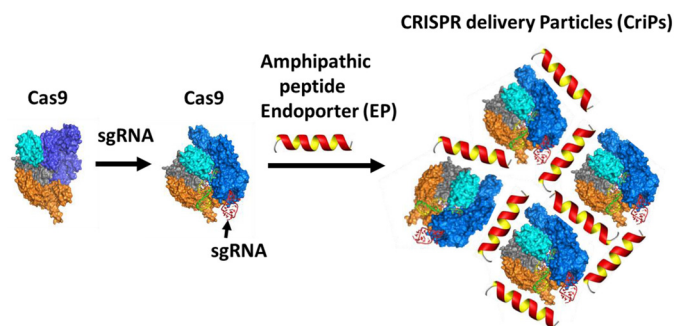


Figure 1. Preparation of CriPs. Purified bacterial Cas9 protein that is carefully processed to remove endotoxin and other contaminants is used for loading of sgRNA. The sgRNA sequence is designed to target a selected gene at a site adjacent to a PAM sequence in the DNA of that target gene. The loaded Cas9–sgRNA nanocomplexes are then coated with an amphipathic peptide, denoted as EP, which is required to mediate uptake of the Cas9–sgRNA complexes into live cells without toxicity or detectable damage.

mediated gene deletion of the GFP gene (*Gfp*) was observed in multiple cell types isolated from GFP transgenic mice, including primary macrophages and primary pre-adipocytes. GFP loss was achieved in about 50% of macrophages and primary pre-adipocytes as determined by flow cytometry analysis, in response to treatment with CriPs targeting *Gfp*. Indels in the *Gfp* genomic locus were confirmed by measurements using a T7 endonuclease I (T7E1) assay. Significant GFP loss was also observed in peritoneal exudate cells (PECs) isolated from GFP transgenic mice after five daily intraperitoneal (i.p.) injections with CriPs targeting *Gfp*, as determined by flow cytometry and confirmed by nucleotide sequencing. Furthermore, deletion of the *Nrip1* gene in white adipocytes by CriPs converted them to a more “brown” adipocyte phenotype, with a remarkable increase of UCP1 expression and no detectable off-target effects as determined by a T7E1 assay.

Results

Design and characterization of CriPs

The goal of the present study was to develop a simple delivery vehicle to effect specific gene deletion via the CRISPR-Cas9–based genome targeting mechanism. For therapeutic applications, we aimed to directly deliver Cas9 protein rather than plasmids that encode the protein to overcome such problems as uncontrolled integration of plasmid DNA into the host genome, unwanted immune responses, and safety issues. Here, we report the preparation of CriPs that can deliver Cas9 protein bound to sgRNA to mediate gene deletion *in vitro* and *in vivo* (Fig. 1). Purified bacterial Cas9 protein that is carefully processed to remove endotoxin and other contaminants is used for loading of sgRNA. The sgRNA sequence is designed to target a selected gene at a site adjacent to a PAM sequence in the DNA of that target gene. The loaded Cas9–sgRNA complexes are then electrostatically complexed with amphipathic EP peptide, which is designed to mediate the uptake of the Cas9–sgRNA complexes into live cells without toxicity or detectable damage. The inert CriPs contain only the three molecular components shown in Fig. 1 (Cas9 protein, sgRNA, and EP). As opposed to gene therapy approaches, no permanent viral vectors or genetic insertions of viral DNA are utilized. Cas9 protein that enters cells through transfection mechanisms lasts no longer than 24 h

Table 1
Size and charge measurements of particles

	Diameter	Polydispersity index	Charge
	<i>nm</i>		<i>mV</i>
EP	0.8 ± 0.2	0.272	18.0 ± 5.5
Cas9	9.3 ± 2.6	0.655	13.9 ± 6.8
Cas9–sgRNA (1:1)	14.3 ± 3.2	0.605	–2.4 ± 3.8
Cas9–sgRNA–EP (1:1:20)	375 ± 47	0.930	6.0 ± 4.4
Cas9–sgRNA–EP (1:1:150)	1098 ± 163	0.580	14.6 ± 6.3
Cas9–sgRNA–EP (1:1:250)	1285 ± 201	0.635	20.7 ± 6.0
Cas9–sgRNA–EP (1:1:20) in DMEM	347 ± 50	0.974	NA ^a
Cas9–sgRNA–EP (1:1:150) in DMEM	1270 ± 192	0.501	NA
Cas9–sgRNA–EP (1:1:250) in DMEM	1489 ± 283	0.387	NA

^a NA, not applicable.

within cells (52). The EP peptide and the sgRNA is also expected to be rapidly degraded within cells. Thus, for *ex vivo* therapeutic approaches such as cell therapy and transplantation of *ex vivo* engineered tissue, Cas9 and other components in CriPs are not present in cells that are implanted. Additionally, unlike RNAi-based approaches, CriP-mediated gene editing lasts for the lifespan of a cell, which allows for less frequent therapeutic administration and less chance of immune response or chronic toxicity.

CriPs with different ratios of EP to Cas9–sgRNA complexes were prepared and measured for their sizes and charges (Table 1). Dynamic light scattering (DLS) measurements showed that the average hydrodynamic sizes of EP, Cas9, and Cas9–sgRNA (1:1) were 0.8 ± 0.2, 9.3 ± 2.6, and 14.3 ± 3.2 nm, respectively. The hydrodynamic size of the CriPs consisting of Cas9–sgRNA–EP (1:1:20) was 375 ± 47 nm. The sizes of the CriPs were further increased when coated with more EPs, suggesting that each particle contains multiple Cas9–sgRNA complexes associated with EP peptides. The sizes of CriPs remained unchanged with dilution in Dulbecco's modified Eagle's medium (DMEM), which mimics the *in vitro* cell culture conditions, suggesting the stability of the particles in the culture media.

ζ potentials of the particles were also measured. Positive charges of +6.0 ± 4.4, +14.6 ± 6.3, and +20.7 ± 6.0 mV were observed for the CriPs loaded with Cas9–sgRNA–EP with a molar ratio at 1:1:20, 1:1:150, and 1:1:250, respectively. The overall positive charge on the surface of the particles could facilitate cellular uptake by interacting with the negatively charged cell membranes.

Deletion of *Gfp* in a macrophage cell line by CriPs

To investigate whether CriPs can efficiently delete genes *in vitro*, we first treated a macrophage cell line, J774A.1, which stably expresses GFP (GFP-J774A.1), with CriPs loaded with sgRNA targeting the *Gfp* gene (*Gfp* sgRNA). The targeting sgRNA directed to *Gfp* is designed to introduce an indel mutation that results in a frameshift and termination of *Gfp* translation. CriPs were incubated with GFP-J774A.1 cells, and the loss of GFP signal was determined by flow cytometry. 7-Amino-actinomycin D (7-AAD) staining was used to distinguish among viable cells and dead cells. Percentages of GFP-negative cells and GFP-positive cells were calculated from the live cells. At 48 h post-treatment, CriPs loaded with *Gfp* sgRNA (Cas9–*Gfp* sgRNA–EP) induced a shift of the GFP signal in 54.0% of the GFP-J774A.1 cells (Fig. 2A and Fig. S1). The shift of the GFP signal rather than the complete loss of GFP after 48 h of treat-

ment was due to the slow degradation of the GFP protein. On day 5 post-treatment, CriPs loaded with *Gfp* sgRNA (Cas9–*Gfp* sgRNA–EP) caused a loss of the GFP signal in 55.2% of the GFP-J774A.1 cells, whereas cells treated with EP only or Cas9–*Gfp* sgRNA only or without any treatment remained GFP-positive in virtually all of the cells (Fig. 2B).

To optimize the gene deletion efficiency of CriPs in GFP-J774A.1 cells, we first determined the relationship between CriP dose and response by changing the concentrations of the Cas9–*Gfp* sgRNA complexes. GFP loss was observed in about 50% of the GFP-J774A.1 cells treated within the range of a 100–300 nM concentration of the Cas9–*Gfp* sgRNA complexes (Fig. 2C). We next tested the effect of the Cas9–sgRNA molar ratio on the gene deletion efficiency. A maximum loss of GFP in 53.3% of the GFP-J774A.1 cells was observed in response to CriPs loaded with a 1:1 molar ratio of Cas9 and *Gfp* sgRNA (Fig. 2D). By assessing the effect of EP concentration on *Gfp* deletion efficiency, a maximum GFP loss in 53.4% of the GFP-J774A.1 cells was observed with 2 μM EP (Fig. 2E), which is the highest concentration of EP that was not associated with detectable cytotoxicity (Fig. S3).

To confirm that the loss of GFP in the GFP-J774A.1 cells was due to genome engineering by the CriPs targeting the *Gfp* gene, the frequency of indel mutations in the *Gfp* genomic locus was determined by a T7E1 assay. The cells treated with CriPs targeting *Gfp* (Cas9–*Gfp* sgRNA–EP) showed 40.4% of indels in the *Gfp* genomic locus, whereas the cells treated with EP alone showed only background noise (Fig. 2F). T7E1 assay usually underestimates the mutation frequencies due to the efficiency of the PCR and the cleavage property of the T7 endonuclease I (53). T7E1 recognizes and cleaves nonperfectly matched DNA at the first, second, or third phosphodiester bond that is upstream of the mismatch. T7E1 cleaves heteroduplex DNA but does not recognize homozygous mutations, completely ignores single polymorphisms (SNPs), and also tends to miss small indels (53).

Comparison of CriPs versus Lipofectamine® RNAiMAX *in vitro*

To compare the gene deletion efficiency by CriPs versus Cas9–sgRNA delivered by commercially available transfect agents, we treated the GFP-J774A.1 cells with either CriPs loaded with *Gfp* sgRNA or Cas9–*Gfp* sgRNA plus Lipofectamine® RNAiMAX. At two time points, 48 h or 5 days post-treatment of Cas9–*Gfp* sgRNA–RNAiMAX, a GFP shift or loss was observed, as determined by flow cytometry in 29.4 and 29.8% of GFP-J774A.1 cells, respectively (Fig. 2G and Fig. S2).

Cas9–sgRNA delivery particles for gene deletion

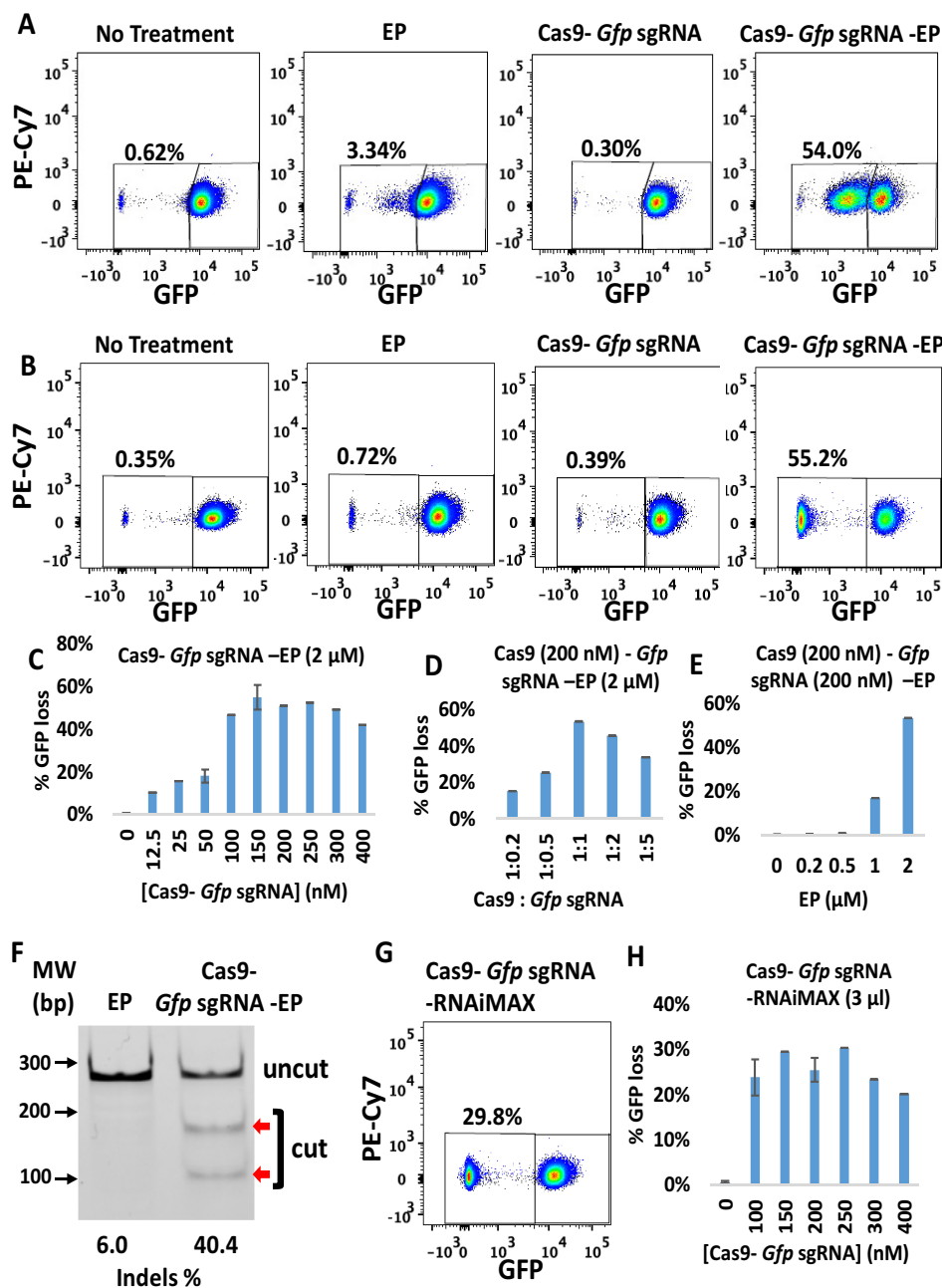


Figure 2. Efficient gene deletion achieved in GFP-J774A.1 cells following treatment with CriPs targeting *Gfp*. At 48 h or at 5 days post-treatment, flow cytometry and T7E1 assays were performed to measure the loss of GFP. *A*, 48 h post-treatment, GFP loss measurements by flow cytometry. *B*, 5 days post-treatment, GFP loss measurements by flow cytometry. Concentrations were as follows: Cas9, 150 nM; *Gfp* sgRNA, 150 nM; EP, 2 μ M. *C*, different concentrations of Cas9–*Gfp* sgRNA (1:1) with 2 μ M EP. *D*, different ratios of Cas9 (200 nM) to *Gfp* sgRNA with 2 μ M EP. *E*, different concentrations of EP with 200 nM Cas9–*Gfp* sgRNA. *F*, percentage indel measurements in *Gfp* genomic DNA isolated from CriP-treated cells versus EP-treated cells by a T7E1 assay (uncut, 292 bp; cut, 179 bp + 113 bp; Cas9, 200 nM; *Gfp* sgRNA, 200 nM; EP, 2 μ M). *G*, flow cytometry data of GFP-expressing J774A.1 cells treated with RNAiMAX-mediated delivery of Cas9–*Gfp* sgRNA at 5 days post-treatment (Cas9, 150 nM; *Gfp* sgRNA, 150 nM). *H*, different concentrations of Cas9–*Gfp* sgRNA (1:1) with RNAiMAX (3 μ l). Error bars, S.E.

Cas9–*Gfp* sgRNA delivered by Lipofectamine® RNAiMAX showed less *Gfp* gene deletion efficiency compared with CriPs, which showed a GFP loss in over 50% of cells (Fig. 1*B*). To optimize the gene deletion efficiency of Cas9–*Gfp* sgRNA delivered by Lipofectamine® RNAiMAX in GFP-J774A.1 cells, the concentrations of the Cas9–*Gfp* sgRNA complexes (Fig. S2, *B* and *D*) and the molar ratio of the Cas9–*Gfp* sgRNA complexes were optimized (Fig. S2, *E* and *F*). A maximum loss of GFP was observed in 20–30% of the GFP-J774A.1 cells treated with the range of a 100–300 nM concentration of the Cas9–*Gfp*

sgRNA complexes at molar ratios of 1:1 to 1:5. These experiments suggest that *Gfp* gene deletion by Cas9–*Gfp* sgRNA delivered using Lipofectamine® RNAiMAX was not as efficient as the CriPs in GFP-J774A.1 cells (Fig. 1 (*A–E*) and Fig. S1).

Gfp deletion in primary white pre-adipocytes from GFP mice

To investigate whether CriPs can efficiently delete genes in primary pre-adipocytes *in vitro*, primary pre-adipocytes were isolated from GFP transgenic heterozygous mice and treated with CriPs loaded with *Gfp* sgRNA or control CriPs loaded with

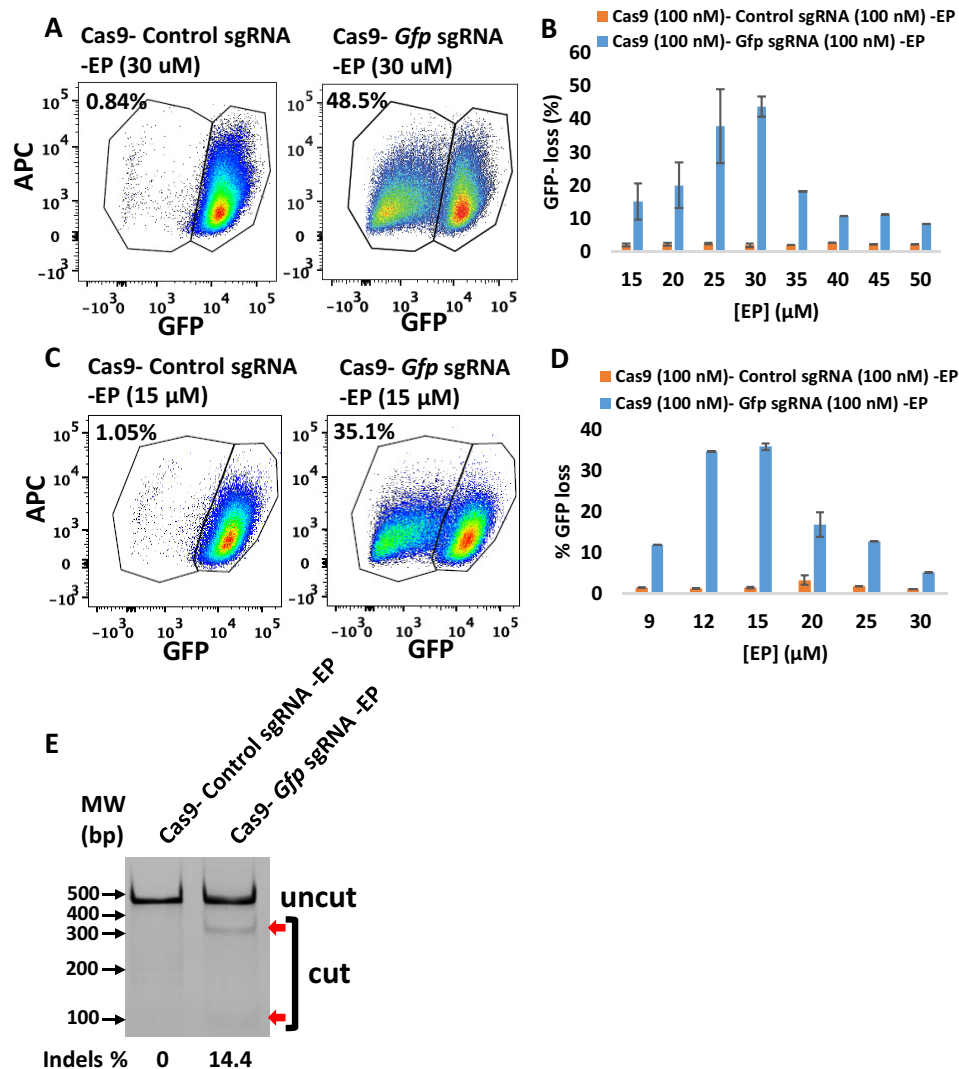


Figure 3. Efficient gene deletion achieved following the treatment with CriPs targeting *Gfp* in primary GFP pre-adipocytes isolated from GFP mice. A and C, flow cytometry data of primary GFP pre-adipocytes treated with CriPs formulated in NEBuffer 3 (A) or PBS (C) (Cas9–sgRNA, 100 nM). B and D, different concentrations of EP with 100 nM of Cas9–sgRNA formulated in NEBuffer 3 (B) or PBS (D). E, percentage indel measurements by a T7E1 assay in genomic DNA isolated from primary GFP pre-adipocytes (uncut, 401 bp; cut, 288 bp + 113 bp). Error bars, S.E.

a control, nontargeting sgRNA (control sgRNA). CriPs were formulated in two different buffer systems, NEBuffer 3 and PBS. CriPs were then incubated with primary GFP white pre-adipocytes. On day 5 post-treatment, the loss of GFP signal was determined by flow cytometry. Formulated in NEBuffer 3 (100 mM NaCl, 50 mM Tris-HCl, 10 mM MgCl₂, 1 mM DTT, pH 7.9), CriPs loaded with *Gfp* sgRNA (Cas9–*Gfp* sgRNA–EP) induced a loss of the GFP signal in 48.5% of the GFP pre-adipocytes, whereas the control CriPs (Cas9–control sgRNA–EP) showed only a background noise of 0.84% of the negative GFP pre-adipocytes (Fig. 3A). To optimize the EP dose that causes the maximum gene deletion efficiency of *Gfp* by CriPs formulated in NEBuffer 3 in the primary GFP pre-adipocytes, the relationship between EP dose and response was determined. A maximum GFP loss was achieved in about 43.7 ± 3.0% of the GFP pre-adipocytes when the Cas9–*Gfp* sgRNA complexes (100 nM) were coated with 30 μM EP (Fig. 3B). Interestingly, the loss of GFP was not complete after 5 days post-transfection, as flow cytometry analysis showed a mixed population of cells that dis-

played either a complete loss of GFP, a shift in GFP loss, or no GFP loss. These variations can possibly be explained by the fact that the GFP transgenic mice likely have multiple *Gfp* transgenes inserted into their genome (54).

When CriPs were formulated in PBS (137 mM NaCl, 2.7 mM KCl, 10 mM Na₂HPO₄, 1.8 mM KH₂PO₄, pH 7.4), a loss of the GFP signal in 35.1% of the GFP pre-adipocytes was observed when treated with CriPs targeting *Gfp* (Cas9–*Gfp* sgRNA–EP), whereas the control CriPs (Cas9–control sgRNA–EP) showed a background of 1.05% loss (Fig. 3C). The dose–response relationship of EP indicated a maximum GFP loss in about 35.8 ± 0.8% of the primary GFP pre-adipocytes treated with the CriPs loaded with the Cas9–*Gfp* sgRNA complexes (100 nM) coated with 15 μM EP (Fig. 3D). Thus, the gene deletion efficiency depends on the formulations of the CriPs in different buffer systems coated with different doses of EP.

To confirm that the loss of the GFP in the primary GFP pre-adipocytes was due to genome engineering by the CriPs targeting the *Gfp* gene, we performed a T7E1 assay to determine the

Cas9–sgRNA delivery particles for gene deletion

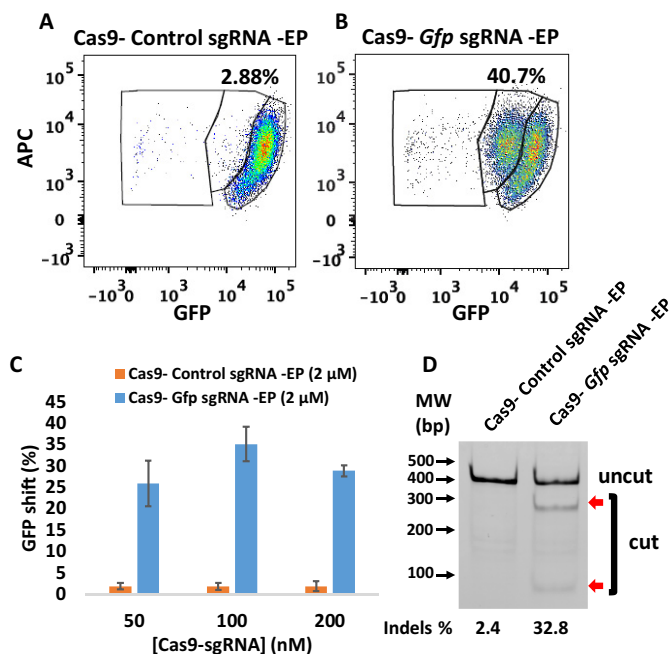


Figure 4. Efficient gene deletion achieved following treatment with CriPs targeting *Gfp* in primary PECs isolated from thioglycollate-injected GFP mice. 5 days post-treatment, flow cytometry and T7E1 assay were performed to measure the loss of GFP. *A* and *B*, flow cytometry data of primary GFP PECs treated with CriPs with a control, nontargeting sgRNA sequence (Cas9–control sgRNA–EP) (*A*) and CriPs targeting *Gfp* (Cas9–*Gfp* sgRNA–EP) (*B*) (Cas9, 100 nM; sgRNA, 100 nM; EP, 2 μM). *C*, different concentrations of Cas9–sgRNA (1:1) with 2 μM EP. *D*, percentage indel measurements in *Gfp* genomic DNA isolated from CriPs-treated primary GFP PECs by a T7E1 assay (uncut, 401 bp; cut, 288 bp + 113 bp; Cas9, 100 nM; sgRNA, 100 nM; EP, 2 μM).

mutation frequency of indels in the *Gfp* genomic locus. Compared with the cells treated with control CriPs, cleaved products were observed in the cells treated with CriPs targeting *Gfp* (Cas9–*Gfp* sgRNA–EP) with a mutation frequency of 14.4% (Fig. 3E). This is probably due to the multiple copies of GFP transgenes inserted into the genome (54) as well as an underestimation caused by the T7E1 assay (53). These results indicate that efficient genome targeting can be achieved by treatment with CriPs in primary pre-adipocytes *in vitro*.

Deletion of *Gfp* in PECs isolated from GFP transgenic mice

To determine the gene deletion efficiency using CriPs in primary GFP PECs, primary PECs that stably express GFP were isolated from GFP transgenic heterozygous mice that had been injected with thioglycollate broth. The PECs were treated with CriPs loaded with *Gfp* sgRNA or control CriPs loaded with control sgRNA. On day 5 post-treatment, the loss of GFP signal was determined by flow cytometry. Compared with control CriPs that showed a background shift of 2.88% (Fig. 4A), CriPs loaded with *Gfp* sgRNA (Cas9–*Gfp* sgRNA–EP) showed a decrease of the GFP signal in 40.7% of the GFP-expressing PECs (Fig. 4B). The relationship between Cas9–sgRNA dose and response indicated a maximum GFP loss of $35.2 \pm 4.0\%$ in the GFP-expressing PECs when the CriPs were loaded with a 100 nM concentration of the Cas9–*Gfp* sgRNA complexes coated with 2 μM EP (Fig. 4C). The T7E1 assay showed a mutation frequency of 32.8% in the *Gfp* genomic DNA isolated from the cells treated with CriPs targeting *Gfp*, compared with a

background of 2.4% in the cells treated with the control CriPs (Fig. 4D).

Deletion of *Gfp* by delivery of CriPs *in vivo* to GFP mice

To determine the ability of CriPs to systemically deliver Cas9–sgRNA RNPs *in vivo* to achieve gene deletion, we administered CriPs to mice by i.p. injections. Shown in Fig. 5A, GFP transgenic heterozygous mice were intraperitoneally injected daily for 5 days with CriPs targeting *Gfp* (CriPs–*Gfp* sgRNA) or with control CriPs (CriPs–control sgRNA). On day 6, mice were sacrificed, and PECs were collected and plated in cell culture. On day 13, flow cytometry was performed to measure the loss of GFP signal. Deep sequencing was also performed to detect the indels in the *Gfp* genomic locus. Measured by flow cytometry, a loss of the GFP signal was observed in the range of 2.9–13.9% of the PECs (average $5.70 \pm 1.07\%$) isolated from 10 GFP transgenic heterozygous mice injected with CriPs–*Gfp* sgRNA. This was significantly greater than the <1% GFP loss we observed in the CriPs–control sgRNA–treated mice (average $0.74 \pm 0.05\%$) (Fig. 5, B and C).

To confirm that the deletion of GFP was due to genome engineering of *Gfp* by CriPs–*Gfp* sgRNA as well as to study the mutation composition of the insertions and deletions in the *Gfp* genomic locus, we performed deep sequencing on the PCR amplicons amplified from the genomic DNA isolated from PECs. Approximately 3% of the target sequences were mutated in the CriPs–*Gfp* sgRNA–injected samples, corroborating the data on the GFP loss measured by flow cytometry shown in Fig. 5B, whereas only a background noise of 0.02% was observed in the CriPs–control sgRNA–injected samples. To study the composition of the mutations in the *Gfp* genomic locus of the CriPs–*Gfp* sgRNA–injected samples, the DNA sequences of the GFP WT and the mutants were aligned (Fig. 5D). The mutants consisted of sequences with insertions and deletions of the bases as well as SNPs in the target site.

Taken together, significant gene deletion of the *Gfp* gene was achieved by i.p. injections of the CriPs targeting *Gfp* *in vivo* in the GFP transgenic heterozygous mice, as determined by both flow cytometry and deep sequencing. This is likely an underestimate of the efficiency because GFP expressing transgenic mice are predicted to have multiple GFP transgenes inserted into their genome (54). A higher genome-engineering efficiency would be expected when editing an endogenous target gene of interest that is present in two copies.

Analysis of immune response in mice injected with CriPs

To examine the possibility of an immune response and systematic inflammation induced by CriPs, we intraperitoneally injected WT mice daily for 5 days with CriPs loaded with a nontargeting sgRNA or PBS as a control. The systemic cytokine profile was analyzed by measuring cytokine levels (IL-1β, IL-4, IL-6, IL-10, IFNγ, and TNFα) in the plasma before injection and then 24 h and 2 weeks after the first injection. The plasma cytokine levels (IL-10 and TNFα) in mice treated with LPS for 1.5 h were also measured to serve as a positive control for the assay (Fig. 6D).

Shown in Fig. 6A, low background levels of inflammatory cytokines were observed before i.p. injection of CriPs and PBS

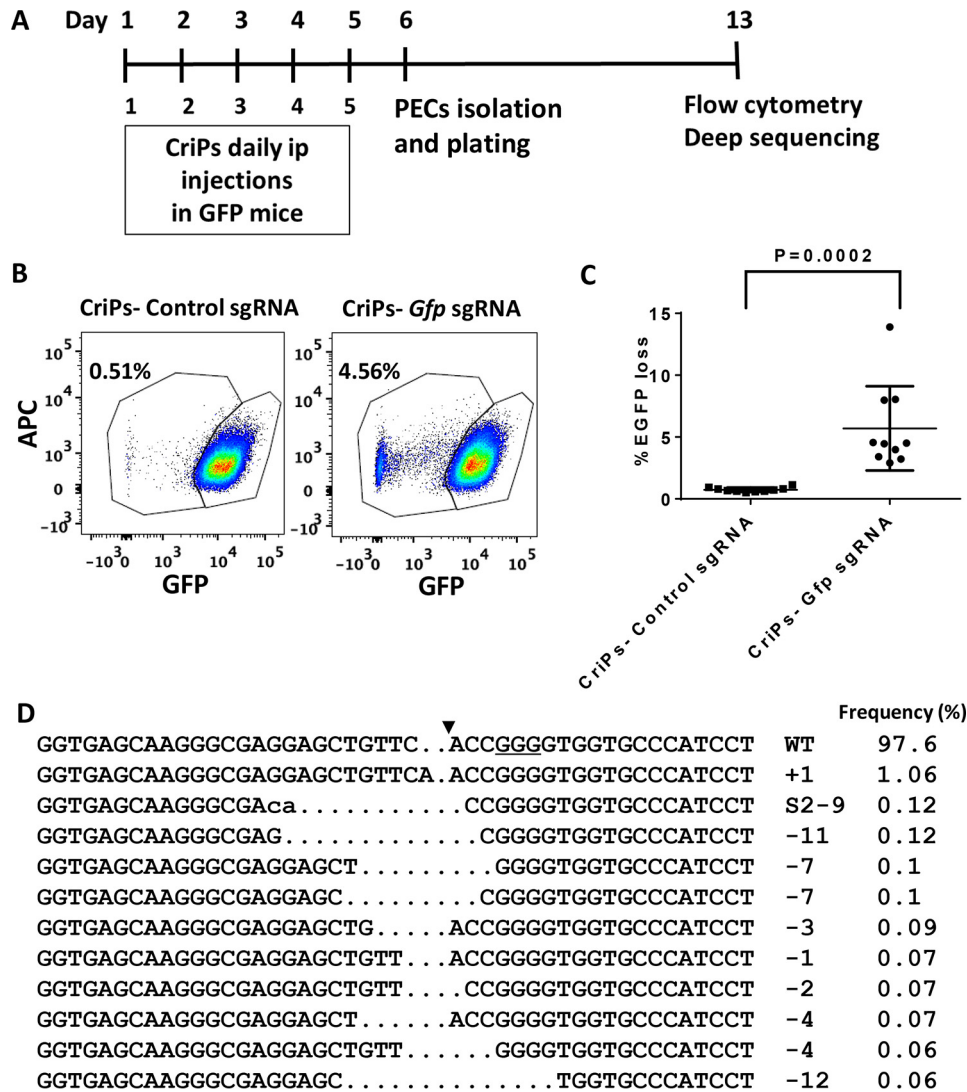


Figure 5. Efficient gene deletion achieved by i.p. injections of CriPs targeting *Gfp* in GFP mice. *A*, timeline of i.p. administration of CriPs to GFP mice. GFP transgenic mice were intraperitoneally injected daily for 5 days with CriPs targeting *Gfp* (CriPs-*Gfp* sgRNA) or control CriPs (CriPs-control sgRNA). On day 6, mice were sacrificed, and PECs were collected and plated in cell culture. On day 13, flow cytometry and deep sequencing were performed to measure the loss of GFP. *B*, flow cytometry data showing GFP loss in mice injected with CriPs-*Gfp* sgRNA or CriPs-control sgRNA. *C*, quantification of flow cytometry data (3–8-week-old GFP male C57BL/6 mice, $n = 10$). *D*, indels in the *Gfp* locus of CriPs-*Gfp* sgRNA-injected samples by deep sequencing. Shown are DNA sequences of the *Gfp* WT and mutants. PAM is underlined. The cleavage site is indicated by an *arrowhead*. The *column on the right* indicates the number and frequencies of inserted (+) or deleted (-) bases or SNPs (S). *Error bars*, S.E.

in mice. Systemic injections of CriPs did not cause an acute (24 h) or a chronic (2 weeks) up-regulation of inflammatory cytokines, such as IL-1 β , IL-4, IL-10, IFN γ , and TNF α , in the plasma (Fig. 6, *B* and *C*), suggesting the absence of a broad immune response upon CriP administration under the conditions of our experiments. Interestingly, the level of IL-6 was increased in the plasma 24 h after the first injection in mice treated with CriPs. IL-6 acts as both a pro-inflammatory cytokine and an anti-inflammatory myokine (55). It can be significantly elevated by many factors, such as exercise (56). More importantly, IL-6 returned to a low background level when it was measured 2 weeks after the first injection. In addition, the low levels of all of the plasma inflammatory cytokines measured 10 days after a total of five injections (2 weeks after the first injection) indicated that CriPs can be administered multiple times systemically *in vivo* without chronic toxicity (Fig. 6*C*).

Deletion of *Nrip1* in primary pre-adipocytes enhances browning

Targeting genes in adipocytes that suppress mitochondrial uncoupling and fatty acid oxidation is a potential strategy to enhance adipocyte browning and energy expenditure (38). Our laboratory has used RNAi-based screens in cultured adipocytes to identify such genes that control insulin sensitivity and energy metabolism (44). An exciting “hit” in these screens of several thousand genes was the nuclear co-repressor *Nrip1* (44), which was also discovered in independent studies in mice (46). NRIP1 interacts with nuclear receptors to suppress their activities to regulate genes that control glucose utilization, mitochondrial function, fatty acid oxidation, and secretion of beneficial factors (44). We and others have found that the depletion of NRIP1 in adipocytes and in mice increased fatty acid oxidation, mitochondrial respiration, insulin sensitivity, and glucose tolerance

Cas9–sgRNA delivery particles for gene deletion

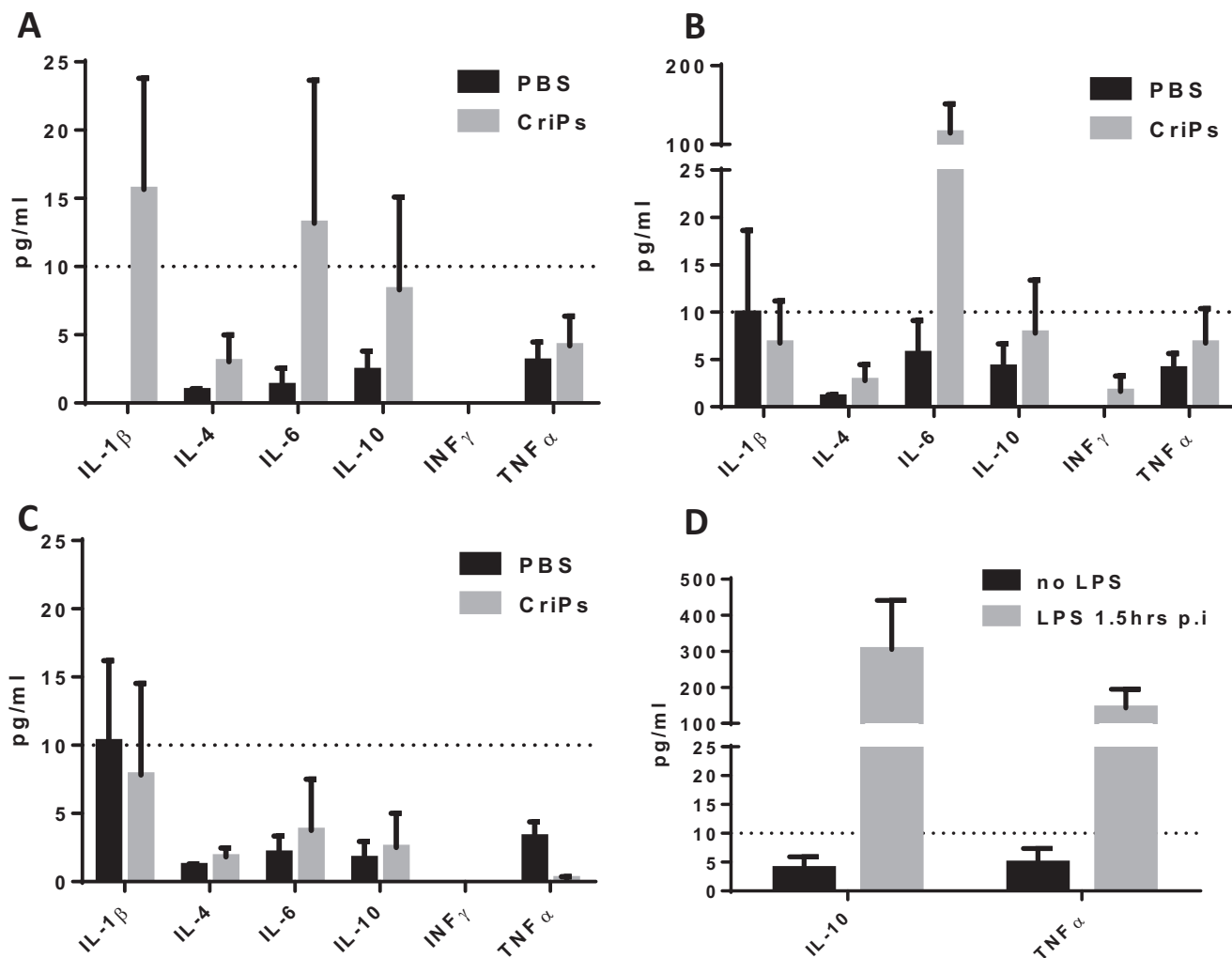


Figure 6. Plasma cytokine levels were measured in mice intraperitoneally injected with CriPs *in vivo*. WT mice were intraperitoneally injected daily for 5 days with PBS or CriPs loaded with a nontargeting sgRNA. Plasma was collected before injection and then 24 h and 2 weeks after the first injection. Plasma cytokine levels (IL-1 β , IL-4, IL-6, IL-10, INF- γ , and TNF α) were measured by Luminex. Plasma cytokine levels were measured before injection (A), 24 h after the first injection (B), and 2 weeks after the first injection (C). D, plasma cytokine levels (IL-10 and TNF α) were also measured in the mice treated with LPS at 1.5 h postinjection (*p.i.*) or without LPS to serve as positive controls for the assay. Data are means \pm S.E. (error bars) ($n = 3-4$).

(44, 46, 57). Therefore, NRIP1 presents a potential therapeutic target for type 2 diabetes and other metabolic disorders.

To investigate whether the *Nrip1* gene can be efficiently deleted in adipocytes and whether the depletion of *Nrip1* can lead to the enhanced expression of genes associated with energy expenditure, such as UCP1, we isolated primary white pre-adipocytes from WT mice and treated them with CriPs loaded with each of four different sgRNAs targeting *Nrip1* (*Nrip1* sgRNA 1, *Nrip1* sgRNA 2, *Nrip1* sgRNA 3, and *Nrip1* sgRNA 4) or control groups (CriPs–control sgRNA, Cas9–EP, EP only, and nontreated). The treated pre-adipocytes were then differentiated to mature adipocytes using a differentiation mixture. On day 8 post-differentiation, cells were collected to measure both the frequency of indels in the *Nrip1* genomic locus by a T7E1 assay and the expression of UCP1 by RT-PCR.

Indicated by a T7E1 assay (Fig. 7A), four CriP formulations, each loaded with a different sgRNA targeting *Nrip1*, showed indels in the *Nrip1* genomic locus with different degrees of mutation frequencies. CriPs loaded with *Nrip1* sequence 3 (*Nrip1* sgRNA 3) demonstrated the highest mutation frequency

of 43.8% in the *Nrip1* genomic locus. More importantly, the deletion of the *Nrip1* gene in the white adipocytes caused the browning of cells, evidenced by increased expression of the uncoupling protein UCP1. Indeed, UCP1 was significantly increased in response to all four CriP formulations loaded with different sgRNAs targeting *Nrip1*. Adipocytes treated with CriPs loaded with the *Nrip1* sgRNA 3, which was most potent in deleting the *Nrip1* gene measured by the T7E1 assay (Fig. 7A), elicited the most marked increase in UCP1 expression (Fig. 7B).

The expression of other thermogenic genes, inflammatory genes, and neurotrophic factors were also measured by RT-PCR in the white adipocytes that had been treated with Cas9–*Nrip1* sgRNA 3–EP and Cas9–control sgRNA–EP. Thermogenic genes involved in adipocyte browning (*Ucp1*, *Cidea*, *Pgc1 α* , *Prdm16*, and *Cpt1b*) were increased with the treatment of CriPs loaded with *Nrip1* sgRNA 3, compared with the control CriPs (Fig. 7C). Neurotrophic factors (*Nrg4*, *Nnat*, and *Nrn1*) were also increased with the treatment of CriPs–*Nrip1* sgRNA 3 (Fig. 7E), whereas inflammatory genes (*Il1 β* , *Il4*, *Il6*, *Il10*, and *Mcp1*) were not changed between CriPs–*Nrip1* sgRNA 3 and CriPs–

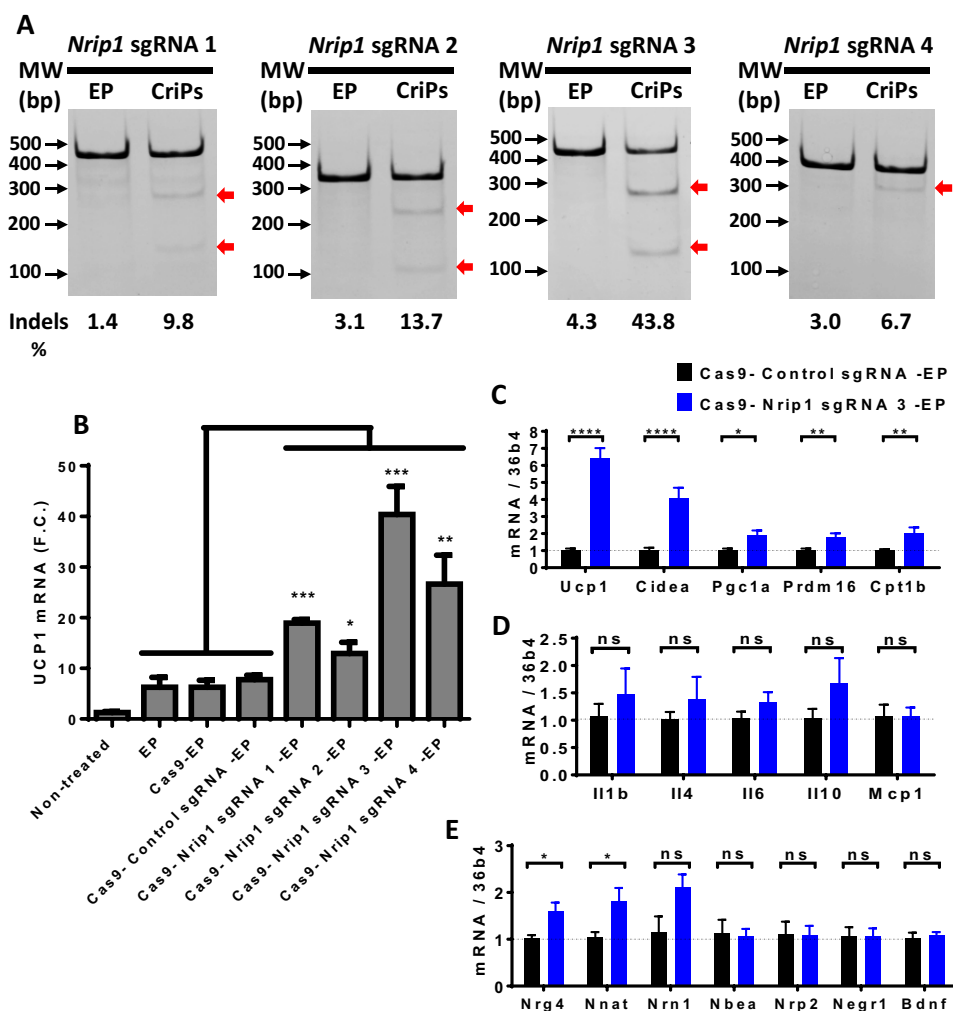


Figure 7. CriPs-mediated *Nrip1* deletion in white adipocytes increases the expression of UCP1. Primary pre-adipocytes were treated with CriPs with each of four different sgRNAs targeting *Nrip1* (*Nrip1* sgRNA 1, *Nrip1* sgRNA 2, *Nrip1* sgRNA 3, and *Nrip1* sgRNA 4) and controls. Pre-adipocytes were then differentiated into mature white adipocytes (Cas9–sgRNA, 100 nM; EP, 25 μ M). **A**, indel detection in *Nrip1* genomic DNA was determined by a T7E1 assay. DNA bands were as follows: *Nrip1* sgRNA 1: uncut, 429 bp; cut, 283 bp + 146 bp; *Nrip1* sgRNA 2: uncut, 334 bp; cut, 223 bp + 111 bp; *Nrip1* sgRNA 3: uncut, 420 bp; cut, 150 bp + 270 bp; *Nrip1* sgRNA 4: uncut, 381 bp; cut, 307 bp + 74 bp. **B**, UCP1 expression was measured by RT-PCR. **C–E**, with the treatment of Cas9–*Nrip1* sgRNA 3–EP and Cas9–control sgRNA–EP, gene expression was measured by RT-PCR. **C**, thermogenic genes; **D**, inflammatory genes; **E**, neurotrophic factors. Error bars, S.E.

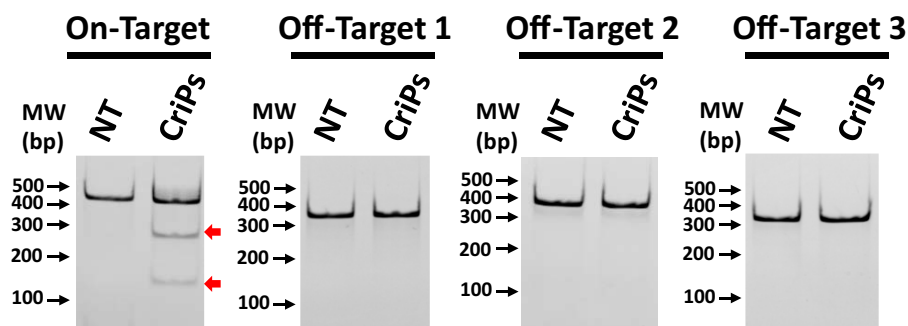
control sgRNA groups (Fig. 7D). Overall, these results indicate that efficient *Nrip1* gene deletion was achieved in white adipocytes treated with CriPs targeting *Nrip1*, and the deletion of the *Nrip1* gene by CriPs converts the white adipocytes to a more “brown” adipocyte phenotype known to be beneficial to whole-body metabolism in mice.

Off-target effects of CriPs targeting *Nrip1* in adipocytes

Primary pre-adipocytes were treated with CriPs loaded with *Nrip1* sgRNA 3, which caused the highest mutation frequency in the *Nrip1* genomic locus and most increased UCP1 in differentiated adipocytes, as indicated in Fig. 7. Differentiated adipocytes were collected to measure the mutation frequencies in the on-target *Nrip1* genomic locus and the off-target genomic sites. All of the off-target sequences contained three mismatch bases compared with the on-target sequence and were located in the intergenic regions. Determined by a T7E1 assay, no obvious off-target effects in the adipocytes treated with CriPs targeting *Nrip1* were observed compared with the nontreated cells (Fig. 8).

Discussion

A key challenge to realizing the potential of CRISPR-Cas9–based therapeutics is the assurance of safe and effective delivery to target cells (6, 9). The major advance of this study is the development of a novel and simple system, CriPs, to efficiently deliver CRISPR-Cas9–based reagents *in vitro* and *in vivo*. CriPs consist of three components (Cas9 protein, sgRNA targeting genes of interest, and the EP peptide), which facilitate transport of large cargoes across cell membranes (Fig. 1). As a therapeutic approach, the direct delivery of Cas9 in protein form enables the swiftest gene editing, as there is no need for transcription or translation of the nuclease (7). Direct delivery of Cas9 protein offers advantages over plasmid delivery and viral delivery, which can display uncontrolled integration of DNA segments into the host genome, unwanted immune responses to the plasmids and virus, and limited packaging capacity (6). It has been shown that the Cas9 protein introduced into cells rapidly degrades within 24 h (52), eliminating immune responses using an *ex vivo* therapeutic approach, where implantation of engi-



Nrip1

On-Target	GGAGTCGAAGAACATCTGCATGG
Off-Target 1	GGAG <u>CTAT</u> AAGAACATCTGCATGG
Off-Target 2	GGAG <u>AT</u> GAAGAACAT <u>G</u> TGCATGG
Off-Target 3	GGAG <u>A</u> AGAACAC <u>CT</u> CTGCATGG

Figure 8. Determination of off-target effects of CriPs targeting *Nrip1* by a T7E1 assay. Primary pre-adipocytes were treated with CriPs with *Nrip1* sgRNA 3. Pre-adipocytes were then differentiated into mature white adipocytes. Top off-target candidate sites were determined by the CHOPCHOP program. Off-target effects were determined by a T7E1 assay. Expected DNA bands cleaved by T7E1 were as follows: on-target: uncut, 420 bp; cut, 270 bp + 150 bp; off-target 1: uncut, 386 bp; cut: 283 bp + 103 bp; off-target 2, uncut: 387 bp; cut, 229 bp + 158 bp; off-target 3: uncut, 352 bp; cut: 182 bp + 170 bp. TGG in *boldface type*, the PAM site. Mismatch sites are *underlined* and in *boldface type*.

neered cells is performed days after gene deletion. Because CriP-mediated gene editing lasts for the lifespan of a cell (*e.g.* up to 10 years for adipocytes) (58), infrequent administration of engineered cell implants would be required to maintain therapeutic efficacy.

Characterized by DLS (Table 1), the CriPs composed of Cas9–sgRNA–EP (1:1:20) showed a hydrodynamic size of 375 ± 47 nm with a positive ζ potential. Compared with Cas9–sgRNA (1:1) alone with a hydrodynamic size of 14.3 ± 3.2 nm, the increase of size indicates the formation of CriPs containing multiple Cas9–sgRNA complexes associated with EP peptides. The overall positive charge on the surface of the particles is predicted to facilitate the cellular uptake by interacting with the negatively charged cell membranes. The sizes and the positive charges of CriPs were further increased when Cas9–sgRNA nanocomplexes were exposed to higher EP concentrations. Interestingly, the unchanged size of CriPs when exposed to DMEM suggests stability of the particles in culture medium.

The present study demonstrates that CriPs facilitate efficient gene deletion of the proof-of-concept gene *Gfp* in multiple cell types, including GFP-J774A.1 cells (Fig. 2), GFP-PECs (Fig. 4), and primary GFP-expressing pre-adipocytes (Fig. 3). We observed GFP loss in about 50% of cells treated with CriPs targeting *Gfp*, detected by flow cytometry analysis (Figs. 2 (A–E), 3 (A–D), and 4 (A–C)) and confirmed by identification of indels in the *Gfp* genomic locus by a T7E1 assay (Figs. 2F, 3E, and 4D). We found that the EP concentration that is optimal for maximal gene deletion is highly cell type–dependent (Figs. 2E and 3 (B and D)). Primary pre-adipocytes require a much higher dose of EP to achieve maximum gene deletion compared with macrophages. On the contrary, high doses of EP are toxic to macrophages but not to primary pre-adipocytes (Fig. S3). Gene deletion efficiency also depends on the formulations of the CriPs in

different buffer systems (Fig. 3, A–D), such as NEBuffer 3 (100 mM NaCl, 50 mM Tris–HCl, 10 mM MgCl₂, 1 mM DTT, pH 7.9) and PBS (137 mM NaCl, 2.7 mM KCl, 10 mM Na₂HPO₄, 1.8 mM KH₂PO₄, pH 7.4), possibly due to salts and pH levels that affect the activity of the Cas9 protein and the electrostatic association of the Cas9–sgRNA nanocomplex and EP. In addition, CriPs demonstrate higher gene deletion efficiency in GFP-J774A.1 cells compared with the Cas9–sgRNA delivered by commercially available Lipofectamine® RNAiMAX (Fig. 2, G and H).

Although many delivery systems have been used to edit genes by Cas9–sgRNA RNPs in cell culture (30, 33), primary cells (15, 19), and local areas of animals, such as inner ear (4, 23), skin (18), tumor (28), muscle (29), and brain (35), systemic delivery of Cas9–sgRNA RNP complexes using a fully nonviral system has not been previously demonstrated. To determine the ability of CriPs to delete genes *in vivo* by systemic delivery, we performed five daily i.p. injections of CriPs targeting *Gfp* (CriPs–*Gfp* sgRNA) or control CriPs (CriPs–control sgRNA) in GFP transgenic heterozygous mice (Fig. 5A). These mice showed a loss of the GFP signal in 2.91–13.90% of the PECs when injected with CriPs–*Gfp* sgRNA, which was significantly higher than the CriPs–control sgRNA–treated group (average $0.74\% \pm 0.05\%$) (Fig. 5, B and C). We also confirmed that about 3% of the target sequences were mutated in the CriPs–*Gfp* sgRNA–injected animals, and the mutants were composed of insertions and deletions of the bases as well as SNPs (Fig. 5D). This is likely an underestimate of the targeting efficiency because GFP transgenic mice likely have multiple *Gfp* transgenes inserted into their genome (54). Taken together, our work demonstrates a simple nonviral genome editing system that delivers Cas9–sgRNA RNPs systemically *in vivo* to achieve significant gene deletion.

Gene editing or deletion in adipose tissue to enhance adipose tissue energy expenditure and fatty acid oxidation through a browning process presents a potential therapeutic approach to alleviate obesity and type 2 diabetes (38, 41). Brown adipocytes not only generate heat but also secrete beneficial factors that enhance glucose tolerance in mice (39, 43). We demonstrate the utility of CriP-mediated gene deletion of *Nrip1* in white adipocytes, demonstrating an induced browning phenotype with remarkably enhanced expression of UCP1, known to uncouple mitochondrial respiration, activate fatty acid oxidation, and improve glucose tolerance (Fig. 7). Using CriPs targeting *Nrip1* in the white adipocytes, we observed a highest mutation frequency of 43.8% in the *Nrip1* genomic locus with *Nrip1* sgRNA 3 measured by a T7E1 assay (Fig. 7A). Adipocytes treated with the CriPs–*Nrip1* sgRNA 3, which were most potent in deleting the *Nrip1* gene, demonstrated the most marked increase in UCP1 expression (Fig. 7B). Other thermogenic genes (*Ucp1*, *Cidea*, *Pgc1 α* , *Prdm16*, and *Cpt1b*) and neurotrophic factors (*Nrg4*, *Nnat*, and *Nrn1*) were also increased (Fig. 7, C and E). In addition, off-target effects in adipocytes treated with CriPs–*Nrip1* sgRNA 3 were not detected by a T7E1 assay (Fig. 8). Thus, the CriPs loaded with sgRNA targeting *Nrip1* provide significant potential for therapeutic development to alleviate metabolic disease.

Experimental procedures

Materials

All chemicals were purchased from Sigma-Aldrich unless otherwise specified and were used as received. Cas9 protein was purchased from PNA BIO, Inc. (Newbury Park, CA). DNA oligonucleotides were purchased from Integrated DNA Technologies Inc. (Coralville, IA). The MEGAshortscript T7 transcription kit, Lipofectamine[®] RNAiMAX, Vybrant MTT cell proliferation assay, and Platinum[™] TaqDNA Polymerase High Fidelity kit were purchased from Thermo Fisher Scientific. BsaI, DraI, T7E1, and NEBuffer 3 were obtained from New England Biolabs Inc. (Ipswich, MA). pUC57–sgRNA expression vector was purchased from Addgene (plasmid 51132) (Cambridge, MA). EP was purchased from Gene Tools (Philomath, OR). The QIAquick PCR purification kit was purchased from Qiagen Inc. (Valencia, CA). 4–20% Mini-Protean TBE gel was purchased from Bio-Rad. 7-AAD was purchased from BD Biosciences. Insulin was purchased from Cell Application (San Diego, CA). Dexamethasone, isobutylmethylxanthine, indomethacin, and lipopolysaccharide (LPS) were purchased from Sigma. Rosiglitazone was purchased from Cayman Chemical (Ann Arbor, MI).

Preparation of sgRNA template and synthesis of sgRNA

sgRNA sequences were designed using sgRNA Designer (59) developed by the Broad Institute and the CHOPCHOP program (60, 61) developed by Harvard University. Templates for sgRNAs were generated by inserting annealed complementary oligonucleotides with the sgRNA sequences into the pUC57–sgRNA expression vector encoding a T7 promoter. The sgRNA templates were linearized by DraI and transcribed *in vitro* using the MEGAshortscript T7 transcription kit according to the manufacturer's instructions. Transcribed sgRNA was resolved

on a 10% denaturing urea-PAGE to check the size and purity. sgRNA sequences are listed in Table S1.

Preparation of the CriPs

Purified bacterial Cas9 protein is processed to remove endotoxin and other contaminants and is used for loading of sgRNA. The powder of Cas9 protein was resuspended in water with 20% glycerol. Cas9 protein and sgRNA were mixed in NEBuffer 3 (100 mM NaCl, 50 mM Tris-HCl, 10 mM MgCl₂, 1 mM DTT, pH 7.9) purchased from New England Biolabs Inc. or PBS (137 mM NaCl, 2.7 mM KCl, 10 mM Na₂HPO₄, 1.8 mM KH₂PO₄, pH 7.4) at 37 °C for 10 min to form nano-size complexes. The loaded Cas9–sgRNA nanocomplexes are then complexed with EP in PBS at room temperature for 15 min to form the final CriPs.

Characterization of the CriPs

The size of CriPs was determined by DLS (laser wavelength 633 nm) using a Malvern Zetasizer Nano-ZS particle size analyzer (Malvern Instruments, Worcestershire, UK). Solvents and buffers were filtered through 0.22- μ m filters before sample preparation. EP (1 mM), Cas9 (1 μ M), Cas9–sgRNA (1 μ M), and CriPs (1 μ M) with different ratios of EP were measured for sizes upon the absence or presence of DMEM (GE Healthcare). ζ potentials of CriPs were also determined with a Malvern Zetasizer Nano-ZS using a Universal “Dip” Cell Kit. Solvents and buffers were filtered through 0.22- μ m filters before sample preparation. A suspension of samples was diluted in 20 mM HEPES buffer for the measurement. Data were analyzed with the Dispersion Technology software (Malvern).

Cell lines and culture

J774A.1 cells were acquired from ATCC (Manassas, VA). J774A.1 cells stably expressing GFP (a gift from Dr. H. Yang, University of Massachusetts Medical School, Worcester, MA) were maintained in DMEM supplemented with 10% (v/v) fetal bovine serum (FBS) (Atlanta Biologicals, Flowery Branch, GA), 100 μ g/ml streptomycin, and 100 units/ml penicillin (Thermo Fisher Scientific). Cell incubations were performed in a water-jacketed 37 °C/5% CO₂ incubator.

In vitro CriPs treatment in GFP-J774A.1 cells

GFP-J774A.1 cells were plated in 12-well plates with 1×10^5 cells/well overnight. Cells were treated with CriPs loaded with *Gfp* sgRNA (Cas9–*Gfp* sgRNA–EP) or controls such as Cas9–*Gfp* sgRNA without EP, EP only, and nontreated. After 24 h, medium containing CriPs and controls was replaced with fresh culture medium. At 48 h or on day 5 post-treatment, flow cytometry analysis was performed to measure the loss of GFP. 7-AAD staining was used to determine live cells and dead cells. The percentages of GFP-negative cells and GFP-positive cells were calculated from the live cells in the flow cytometry analysis. Indels in the *Gfp* genomic locus were measured by a T7E1 assay.

Transfection of GFP-J774A.1 with Cas9–sgRNA using RNAiMAX

GFP-J774A.1 cells were plated in 12-well plates with 1×10^5 cells/well overnight. Cells were treated with Cas9–*Gfp* sgRNA

Cas9–sgRNA delivery particles for gene deletion

complexes delivered by Lipofectamine® RNAiMAX or controls such as Cas9–*Gfp* sgRNA without RNAiMAX, RNAiMAX only, and nontreated. After 24 h, cells were fed with fresh culture medium. At 48 h or on day 5 post-treatment, flow cytometry analysis was performed to measure the loss of GFP. 7-AAD staining was used to determine live cells and dead cells. The percentages of GFP-negative cells and of GFP-positive cells were calculated from the live cells analyzed by flow cytometry.

Animals

All mice were purchased from Jackson Laboratory. WT mice (C57BL/6J) and GFP transgenic heterozygous mice (C57BL/6-Tg(UBC-GFP)30Scha/J) were used for the experiments. Mice were housed on a 12-h light/dark schedule and had free access to water and food. All procedures involving animals were approved by the institutional animal care and use committee at the University of Massachusetts Medical School.

Isolation of primary PECs from GFP transgenic mice

Ten-week-old GFP transgenic heterozygous mice were intraperitoneally injected with 4% thioglycollate broth (Sigma-Aldrich). Five days following injection, the mice were sacrificed, and the peritoneal cavity was washed with 5 ml of ice-cold PBS to isolate PECs. Peritoneal fluid was filtered through a 70- μ m pore nylon mesh and centrifuged at 1200 rpm for 10 min. The pellet was first treated with red blood cell lysis buffer (8.3 g of NH_4Cl , 1.0 g of KHCO_3 , and 0.037 g of EDTA dissolved in 1 liter of water) and resuspended in DMEM supplemented with 10% (v/v) FBS, 100 $\mu\text{g}/\text{ml}$ streptomycin, and 100 units/ml penicillin.

In vitro CriPs treatment of primary GFP PECs

Primary GFP PECs isolated from GFP transgenic mice were plated in 12-well plates with 5×10^5 cells/well overnight. Cells were treated with CriPs loaded with *Gfp* sgRNA or control sgRNA. After 24 h, cells were fed with fresh culture medium. On day 5 post-treatment, flow cytometry analysis was performed to measure the loss of GFP. 7-AAD staining was used to determine live cells and dead cells. The percentages of GFP-negative cells and GFP-positive cells were calculated from the live cells analyzed by flow cytometry. Indels in the *Gfp* genomic locus were measured by a T7E1 assay.

Culture of primary white pre-adipocytes from mice

Three-week-old GFP transgenic heterozygous mice or WT mice were sacrificed, and inguinal subcutaneous fat pads were dissected out and placed into Hanks' balanced salt solution (without Ca^{2+}) with 3% BSA. Tissues were minced with scissors to ~3–5-mm pieces. Tissues were digested in collagenase D solution (2 mg/ml collagenase D in Hanks' balanced salt solution with 3% BSA) in a 37 °C water bath shaker for 1 h with short vortex every 10–15 min. Samples were inactivated with 10% FBS, filtered through a 100- μ m mesh, and centrifuged at $600 \times g$ for 5 min. The stromal vascular fraction pellet was resuspended in red blood cell lysis buffer for 5 min and centrifuged again at $600 \times g$ for 5 min. Cell pellet was resuspended in DMEM/F-12 medium with 10% FBS and 1% streptomycin/penicillin, filtered through 40- μ m mesh, and plated. Medium was replaced every 2 days until cells reached 100% confluence

before differentiation. Cells were differentiated by adding the differentiation mixture (5 $\mu\text{g}/\text{ml}$ insulin, 1 μM dexamethasone, 0.5 mM isobutylmethylxanthine, 60 μM indomethacin, 1 μM rosiglitazone). After 48 h, the medium was changed to only include 1 μM rosiglitazone and 5 $\mu\text{g}/\text{ml}$ insulin. After another 48 h, the medium was changed to include 5 $\mu\text{g}/\text{ml}$ insulin only. On day 5 post-differentiation, the cells are considered fully differentiated.

Treatment of mouse primary white pre-adipocytes with CriPs

Gfp target gene—Primary GFP white pre-adipocytes were isolated from GFP transgenic heterozygous mice and plated in 12-well plates with 8×10^4 cells/well overnight. Cells were treated with CriPs loaded with *Gfp* sgRNA or control CriPs loaded with control sgRNA. After 24 h, cells were fed with fresh culture medium. On day 5 post-treatment, flow cytometry analysis was performed to measure the loss of GFP. 7-AAD staining was used to determine live cells and dead cells. The percentages of GFP-negative cells and GFP-positive cells were calculated from the live cells analyzed by flow cytometry. Indels in the *Gfp* genomic locus were measured by a T7E1 assay.

Nrip1 target gene—Primary white pre-adipocytes were isolated from WT mice and plated in 12-well plates with 8×10^4 cells/well overnight. Cells were treated with CriPs loaded with each of four different sgRNAs targeting *Nrip1* (*Nrip1* sgRNA 1, *Nrip1* sgRNA 2, *Nrip1* sgRNA 3, and *Nrip1* sgRNA 4) or control groups (CriPs–control sgRNA, Cas9–EP, EP only, and nontreated) (Cas9–sgRNA, 100 nM; EP, 25 μM). After 24 h, cells were fed with fresh culture medium. Once the pre-adipocytes reached 100% confluence, they were differentiated to adipocytes with the differentiation mixture. On day 8 post-differentiation, cells were collected to measure indels in the *Nrip1* genomic locus by a T7E1 assay.

Gene expression of white adipocytes after *Nrip1* CriP deletion

Primary white pre-adipocytes were isolated from WT mice and treated with CriPs loaded with each of the four sgRNAs targeting *Nrip1* (*Nrip1* sgRNA 1, *Nrip1* sgRNA 2, *Nrip1* sgRNA 3, and *Nrip1* sgRNA 4) or control groups (CriPs–control sgRNA, Cas9–EP, EP only, and nontreated) (Cas9–sgRNA, 100 nM; EP, 25 μM). Once the pre-adipocytes reached 100% confluence, they were differentiated to adipocytes with the differentiation mixture. On day 8 post-differentiation, cells were collected to measure the expression of UCP1 by RT-PCR. The expression of other thermogenic genes, inflammatory genes, and neurotropic factors was also measured in cells treated with CriPs loaded with *Nrip1* sgRNA 3 or control sgRNA by RT-PCR.

Off-target effects of CriPs targeting *Nrip1*

Primary white pre-adipocytes were treated with CriPs (Cas9–sgRNA, 100 nM; EP, 25 μM) loaded with *Nrip1* sgRNA 3. Pre-adipocytes were then differentiated to mature white adipocytes. On day 8 post-differentiation, cells were collected to measure indels in the *Nrip1* genomic locus or at the off-target sites by a T7E1 assay. Sequences targeting the top off-target candidate sites were determined by the CHOPCHOP program (60, 61). Expected DNA bands cleaved by T7E1 were as follows:

on-target: uncut, 420 bp; cut, 270 bp + 150 bp; off-target 1: uncut, 386 bp; cut, 283 bp + 103 bp; off-target 2: uncut, 387 bp; cut, 229 bp + 158 bp; off-target 3: uncut, 352 bp; cut, 182 bp + 170 bp. Off-target sequences are listed in Table S3.

Cytotoxicity assay post-CriP treatment in vitro

The cytotoxicity of Cas9–sgRNA coated with different EP concentrations in different cell types (J774A.1 cells, PECs, and primary white pre-adipocytes) was examined by the Vybrant MTT cell proliferation assay. Cells were treated with Cas9–sgRNA (100 nM) coated with different concentrations of EP. After 24 h, the particle-containing medium was replaced by fresh culture medium. After another 24 h, the medium was changed to fresh culture medium without phenol red, and 10 μ l of 12 mM MTT stock solution was added to each well. The plate was incubated for an additional 4 h at 37 °C in a humidified CO₂ incubator. Following the 4-h incubation, 100 μ l of the SDS-HCl solution was added to each well and incubated overnight. The absorbance of the colored formazan product was recorded at 570 nm using a microplate reader (Tecan Group Ltd.) and normalized to the control group with no treatment. An average of three determinations were made.

In vivo treatment of GFP transgenic mice with CriPs

GFP transgenic heterozygous mice (male, 3–8 weeks old) were intraperitoneally injected daily for 5 days with CriPs loaded with *Gfp* sgRNA or control sgRNA. The CriPs contained 0.9 nmol of Cas9 protein, 0.9 nmol of sgRNA, and 20 nmol of EP for each injection. On day 6, mice were sacrificed, and the peritoneal cavity was washed with 5 ml of ice-cold PBS to isolate PECs. The cells were plated in the medium (DMEM supplemented with 10% (v/v) FBS, 100 μ g/ml streptomycin, and 100 units/ml penicillin) to enrich for macrophages. Fresh medium was added every 48 h. On day 13 (8 days after the last injection), adhered cells were collected. Flow cytometry analysis was performed to measure the loss of GFP. 7-AAD staining was used to determine live cells and dead cells. The percentages of GFP-negative cells and GFP-positive cells were calculated from the live cells. Genomic DNAs were also collected for detecting indels by deep sequencing.

Deep sequencing of PECs after in vivo CriP treatment

PECs were isolated from GFP mice intraperitoneally injected with CriPs–*Gfp* sgRNA and CriPs–control sgRNA. The *Gfp* genomic region of the CriPs–*Gfp* sgRNA target sequence was amplified by PCR using the PlatinumTM TaqDNA Polymerase High Fidelity kit according to the manufacturer's protocol. The amplicons were purified using the QIAquick PCR purification kit. Libraries were made from the purified amplicons and sequenced on the Illumina MiSeq instrument (300-bp paired end) by the University of Massachusetts Medical School Deep Sequencing Core Facility. Reads were mapped to the *Gfp* reference sequence, and insertion/deletion/SNP mutations were determined by the CRISPR-Dav program (62).

Plasma cytokine levels in mice treated with CriPs in vivo

WT mice (male, 20 weeks old) were intraperitoneally injected daily for 5 days with CriPs loaded with a nontargeting

sgRNA (*Gfp* sgRNA) or PBS. The CriPs contained 0.9 nmol of Cas9 protein, 0.9 nmol of sgRNA, and 20 nmol of EP for each injection. Serum was collected at three time points: before injection, 24 h after the first injection, and 2 weeks after the first injection. Plasma cytokine levels (IL-1 β , IL-4, IL-6, IL-10, IFN γ , of TNF α) were measured using a Luminex multiplex assays on a Lincplex instrument by the National Mouse Metabolic Phenotyping Center at the University of Massachusetts Medical School. The assays were performed according to the manufacturer's recommended procedures. Plasma cytokine levels (IL-10 and TNF α) were also measured in mice treated with LPS for 1.5 h or without LPS to serve as positive controls for the assay. Data are means \pm S.E. ($n = 3–4$ mice/group).

T7E1 assay

Cells were lysed in cell lysis buffer (1 M KCl, 1 M MgCl₂, 1 M Tris base, pH 8.3, 0.45% Nonidet P-40, 0.45% Tween 20, 0.1 mg/ml proteinase K) and then used as templates in PCRs to amplify the targeted genomic loci using the PlatinumTM TaqDNA Polymerase High Fidelity kit according to the manufacturer's protocol. PCR products were purified using the QIAquick PCR purification kit and quantified by Nanodrop. Purified PCR products (200 ng) were mixed with 2 μ l of 10 \times NEBuffer 2 (New England Biolabs, Inc.) up to a total volume of 19 μ l and denatured and then re-annealed with thermocycling at 95 °C for 5 min, 95 to 85 °C at 2 °C/s, 85 to 20 °C at 0.2 °C/s. The re-annealed DNA was incubated with 1 μ l of T7E1 at 37 °C for 15 min. The reaction was stopped by adding 1.5 μ l of 0.25 M EDTA and analyzed on a 4–20% Mini-Protean TBE gel electrophoresed for 1.5 h at 100 V and then stained with ethidium bromide. The frequency of indels was calculated based on the band intensities quantified using Image Lab (Bio-Rad). The intensities of the cleaved bands were divided by the total intensities of all bands (uncleaved + cleaved) to determine the frequency of indels to estimate gene modification levels. Primer sequences are listed in Tables S2 and S4.

Author contributions—Y. S. designed the study, performed the research, analyzed the data, and wrote the manuscript. M. P. C. designed the study and wrote the manuscript. J. L. C. performed the experiments and analyzed the data. S. M. N. performed the experiments, analyzed the data, and revised the manuscript. M. K., B. Y., F. H., and E. T. performed the experiments. Y. J. K. E. analyzed the deep sequencing data. X. H., R. H. F., and J. K. K. performed the Luminex multiplex assays. All authors reviewed and edited the manuscript.

Acknowledgments—We thank the members of our laboratory group for excellent discussion of the data in this paper. We appreciate the help of the staff of the Flow Cytometry Core Facility, the Deep Sequencing Core Facility, and the National Mouse Metabolic Phenotyping Center (MMPC) at the University of Massachusetts Medical School. We thank Dr. Gang Han for use of the Malvern Zetasizer Nano-ZS particle size analyzer. We also thank Dr. H. Yang for GFP-expressing J774A.1 cells.

Cas9–sgRNA delivery particles for gene deletion

References

- Hsu, P. D., Lander, E. S., and Zhang, F. (2014) Development and applications of CRISPR-Cas9 for genome engineering. *Cell* **157**, 1262–1278 [CrossRef Medline](#)
- Komor, A. C., Badran, A. H., and Liu, D. R. (2017) CRISPR-based technologies for the manipulation of eukaryotic genomes. *Cell* **169**, 559 [CrossRef Medline](#)
- Eyquem, J., Mansilla-Soto, J., Giavridis, T., van der Stegen, S. J., Hamieh, M., Cunanan, K. M., Odak, A., Gönen, M., and Sadelain, M. (2017) Targeting a CAR to the TRAC locus with CRISPR/Cas9 enhances tumour rejection. *Nature* **543**, 113–117 [CrossRef Medline](#)
- Gao, X., Tao, Y., Lamas, V., Huang, M., Yeh, W. H., Pan, B., Hu, Y. J., Hu, J. H., Thompson, D. B., Shu, Y., Li, Y., Wang, H., Yang, S., Xu, Q., Polley, D. B., Liberman, M. C., Kong, W. J., Holt, J. R., Chen, Z. Y., and Liu, D. R. (2018) Treatment of autosomal dominant hearing loss by *in vivo* delivery of genome editing agents. *Nature* **553**, 217–221 [Medline](#)
- Ran, F. A., Hsu, P. D., Wright, J., Agarwala, V., Scott, D. A., and Zhang, F. (2013) Genome engineering using the CRISPR-Cas9 system. *Nat. Protoc.* **8**, 2281–2308 [CrossRef Medline](#)
- Wang, H. X., Li, M., Lee, C. M., Chakraborty, S., Kim, H. W., Bao, G., and Leong, K. W. (2017) CRISPR/Cas9-based genome editing for disease modeling and therapy: challenges and opportunities for nonviral delivery. *Chem. Rev.* **117**, 9874–9906 [CrossRef Medline](#)
- Glass, Z., Lee, M., Li, Y., and Xu, Q. (2018) Engineering the delivery system for CRISPR-based genome editing. *Trends Biotechnol.* **36**, 173–185 [CrossRef Medline](#)
- Li, L., He, Z. Y., Wei, X. W., Gao, G. P., and Wei, Y. Q. (2015) Challenges in CRISPR/CAS9 Delivery: potential roles of nonviral vectors. *Hum. Gene Ther.* **26**, 452–462 [CrossRef Medline](#)
- Li, L., Hu, S., and Chen, X. (2018) Non-viral delivery systems for CRISPR/Cas9-based genome editing: challenges and opportunities. *Biomaterials* **171**, 207–218 [CrossRef Medline](#)
- Tabebordbar, M., Zhu, K., Cheng, J. K. W., Chew, W. L., Widrick, J. J., Yan, W. X., Maesner, C., Wu, E. Y., Xiao, R., Ran, F. A., Cong, L., Zhang, F., Vandenbergh, L. H., Church, G. M., and Wagers, A. J. (2016) *In vivo* gene editing in dystrophic mouse muscle and muscle stem cells. *Science* **351**, 407–411 [CrossRef Medline](#)
- Wang, D., Mou, H., Li, S., Li, Y., Hough, S., Tran, K., Li, J., Yin, H., Anderson, D. G., Sontheimer, E. J., Weng, Z., Gao, G., and Xue, W. (2015) Adenovirus-mediated somatic genome editing of Pten by CRISPR/Cas9 in mouse liver in spite of Cas9-specific immune responses. *Hum. Gene Ther.* **26**, 432–442 [CrossRef Medline](#)
- Swiech, L., Heidenreich, M., Banerjee, A., Habib, N., Li, Y., Trombetta, J., Sur, M., and Zhang, F. (2015) *In vivo* interrogation of gene function in the mammalian brain using CRISPR-Cas9. *Nat. Biotechnol.* **33**, 102–106 [CrossRef Medline](#)
- Platt, R. J., Chen, S., Zhou, Y., Yim, M. J., Swiech, L., Kempton, H. R., Dahlman, J. E., Parnas, O., Eisenhaure, T. M., Jovanovic, M., Graham, D. B., Jhunjhunwala, S., Heidenreich, M., Xavier, R. J., Langer, R., Anderson, D. G., *et al.* (2014) CRISPR-Cas9 knockin mice for genome editing and cancer modeling. *Cell* **159**, 440–455 [CrossRef Medline](#)
- Wu, Z., Yang, H., and Colosi, P. (2010) Effect of genome size on AAV vector packaging. *Mol. Ther.* **18**, 80–86 [CrossRef Medline](#)
- Schumann, K., Lin, S., Boyer, E., Simeonov, D. R., Subramaniam, M., Gate, R. E., Haliburton, G. E., Ye, C. J., Bluestone, J. A., Doudna, J. A., and Marson, A. (2015) Generation of knock-in primary human T cells using Cas9 ribonucleoproteins. *Proc. Natl. Acad. Sci. U.S.A.* **112**, 10437–10442 [CrossRef Medline](#)
- Lin, S., Staahl, B. T., Alla, R. K., and Doudna, J. A. (2014) Enhanced homology-directed human genome engineering by controlled timing of CRISPR/Cas9 delivery. *Elife* **3**, e04766 [CrossRef Medline](#)
- Gundry, M. C., Brunetti, L., Lin, A., Mayle, A. E., Kitano, A., Wagner, D., Hsu, J. I., Hoegenauer, K. A., Rooney, C. M., Goodell, M. A., and Nakada, D. (2016) Highly efficient genome editing of murine and human hematopoietic progenitor cells by CRISPR/Cas9. *Cell Rep.* **17**, 1453–1461 [CrossRef Medline](#)
- Wu, W., Lu, Z., Li, F., Wang, W., Qian, N., Duan, J., Zhang, Y., Wang, F., and Chen, T. (2017) Efficient *in vivo* gene editing using ribonucleoproteins in skin stem cells of recessive dystrophic epidermolysis bullosa mouse model. *Proc. Natl. Acad. Sci. U.S.A.* **114**, 1660–1665 [CrossRef Medline](#)
- Hultquist, J. F., Schumann, K., Woo, J. M., Mangano, L., McGregor, M. J., Doudna, J., Simon, V., Krogan, N. J., and Marson, A. (2016) A Cas9 ribonucleoprotein platform for functional genetic studies of HIV-host interactions in primary human T cells. *Cell Rep.* **17**, 1438–1452 [CrossRef Medline](#)
- Li, D., Qiu, Z., Shao, Y., Chen, Y., Guan, Y., Liu, M., Li, Y., Gao, N., Wang, L., Lu, X., Zhao, Y., and Liu, M. (2013) Heritable gene targeting in the mouse and rat using a CRISPR-Cas system. *Nat. Biotechnol.* **31**, 681–683 [CrossRef Medline](#)
- Xue, W., Chen, S., Yin, H., Tammela, T., Papagiannakopoulos, T., Joshi, N. S., Cai, W., Yang, G., Bronson, R., Crowley, D. G., Zhang, F., Anderson, D. G., Sharp, P. A., and Jacks, T. (2014) CRISPR-mediated direct mutation of cancer genes in the mouse liver. *Nature* **514**, 380–384 [CrossRef Medline](#)
- Yin, H., Xue, W., Chen, S., Bogorad, R. L., Benedetti, E., Grompe, M., Kotliansky, V., Sharp, P. A., Jacks, T., and Anderson, D. G. (2014) Genome editing with Cas9 in adult mice corrects a disease mutation and phenotype. *Nat. Biotechnol.* **32**, 551–553 [CrossRef Medline](#)
- Zuris, J. A., Thompson, D. B., Shu, Y., Guilinger, J. P., Bessen, J. L., Hu, J. H., Maeder, M. L., Joung, J. K., Chen, Z. Y., and Liu, D. R. (2015) Cationic lipid-mediated delivery of proteins enables efficient protein-based genome editing *in vitro* and *in vivo*. *Nat. Biotechnol.* **33**, 73–80 [CrossRef Medline](#)
- Finn, J. D., Smith, A. R., Patel, M. C., Shaw, L., Youniss, M. R., van Heteren, J., Dirstine, T., Ciullo, C., Lescarbeau, R., Seitzer, J., Shah, R. R., Shah, A., Ling, D., Growe, J., Pink, M., *et al.* (2018) A single administration of CRISPR/Cas9 lipid nanoparticles achieves robust and persistent *in vivo* genome editing. *Cell Rep.* **22**, 2227–2235 [CrossRef Medline](#)
- Miller, J. B., Zhang, S., Kos, P., Xiong, H., Zhou, K., Perelman, S. S., Zhu, H., and Siegwart, D. J. (2017) Non-viral CRISPR/Cas gene editing *in vitro* and *in vivo* enabled by synthetic nanoparticle co-delivery of Cas9 mRNA and sgRNA. *Chem. Int. Ed. Engl.* **56**, 1059–1063 [CrossRef Medline](#)
- Jiang, C., Mei, M., Li, B., Zhu, X., Zu, W., Tian, Y., Wang, Q., Guo, Y., Dong, Y., and Tan, X. (2017) A non-viral CRISPR/Cas9 delivery system for therapeutically targeting HBV DNA and psc9 *in vivo*. *Cell Res.* **27**, 440–443 [CrossRef Medline](#)
- Wang, M., Zuris, J. A., Meng, F., Rees, H., Sun, S., Deng, P., Han, Y., Gao, X., Pouli, D., Wu, Q., Georgakoudi, I., Liu, D. R., and Xu, Q. (2016) Efficient delivery of genome-editing proteins using bio-reducible lipid nanoparticles. *Proc. Natl. Acad. Sci. U.S.A.* **113**, 2868–2873 [CrossRef Medline](#)
- Sun, W., Ji, W., Hall, J. M., Hu, Q., Wang, C., Beisel, C. L., and Gu, Z. (2015) Self-assembled DNA nanoclews for the efficient delivery of CRISPR-Cas9 for genome editing. *Angew. Chem. Int. Ed. Engl.* **54**, 12029–12033 [CrossRef Medline](#)
- Lee, K., Conboy, M., Park, H. M., Jiang, F., Kim, H. J., Dewitt, M. A., Mackley, V. A., Chang, K., Rao, A., Skinner, C., Shobha, T., Mehdipour, M., Liu, H., Huang, W. C., Lan, F., *et al.* (2017) Nanoparticle delivery of Cas9 ribonucleoprotein and donor DNA *in vivo* induces homology-directed DNA repair. *Nat. Biomed. Eng.* **1**, 889–901 [CrossRef Medline](#)
- Mout, R., Ray, M., Yesilbag Tonga, G., Lee, Y. W., Tay, T., Sasaki, K., and Rotello, V. M. (2017) Direct cytosolic delivery of CRISPR/Cas9-ribonucleoprotein for efficient gene editing. *ACS Nano* **11**, 2452–2458 [CrossRef Medline](#)
- Kang, Y. K., Kwon, K., Ryu, J. S., Lee, H. N., Park, C., and Chung, H. J. (2017) Nonviral genome editing based on a polymer-derivatized CRISPR nanocomplex for targeting bacterial pathogens and antibiotic resistance. *Bioconjug. Chem.* **28**, 957–967 [CrossRef Medline](#)
- Ramakrishna, S., Kwaku Dad, A. B., Bloor, J., Gopalappa, R., Lee, S. K., and Kim, H. (2014) Gene disruption by cell-penetrating peptide-mediated delivery of Cas9 protein and guide RNA. *Genome Res.* **24**, 1020–1027 [CrossRef Medline](#)

33. Cho, S. W., Kim, S., Kim, J. M., and Kim, J. S. (2013) Targeted genome engineering in human cells with the Cas9 RNA-guided endonuclease. *Nat. Biotechnol.* **31**, 230–232 [CrossRef Medline](#)
34. Wang, H. X., Song, Z., Lao, Y. H., Xu, X., Gong, J., Cheng, D., Chakraborty, S., Park, J. S., Li, M., Huang, D., Yin, L., Cheng, J., and Leong, K. W. (2018) Nonviral gene editing via CRISPR/Cas9 delivery by membrane-disruptive and endosomolytic helical polypeptide. *Proc. Natl. Acad. Sci. U.S.A.* **115**, 4903–4908 [CrossRef Medline](#)
35. Staahl, B. T., Benekareddy, M., Coulon-Bainier, C., Banfal, A. A., Floor, S. N., Sabo, J. K., Urnes, C., Munares, G. A., Ghosh, A., and Doudna, J. A. (2017) Efficient genome editing in the mouse brain by local delivery of engineered Cas9 ribonucleoprotein complexes. *Nat. Biotechnol.* **35**, 431–434 [CrossRef Medline](#)
36. Centers for Disease Control and Prevention (2017) *National Diabetes Statistics Report 2017*, Centers for Disease Control and Prevention, United States Department of Health and Human Services, Atlanta, GA
37. Spiegelman, B. M. (2013) Banting Lecture 2012: Regulation of adipogenesis: toward new therapeutics for metabolic disease. *Diabetes* **62**, 1774–1782 [CrossRef Medline](#)
38. Harms, M., and Seale, P. (2013) Brown and beige fat: development, function and therapeutic potential. *Nat. Med.* **19**, 1252–1263 [CrossRef Medline](#)
39. Villarroya, F., and Giral, M. (2015) The beneficial effects of brown fat transplantation: further evidence of an endocrine role of brown adipose tissue. *Endocrinology* **156**, 2368–2370 [CrossRef Medline](#)
40. Villarroya, J., Cereijo, R., and Villarroya, F. (2013) An endocrine role for brown adipose tissue? *Am. J. Physiol. Endocrinol. Metab.* **305**, E567–E572 [CrossRef Medline](#)
41. Chondronikola, M., Volpi, E., Børshiem, E., Porter, C., Annamalai, P., Enerbäck, S., Lidell, M. E., Saraf, M. K., Labbe, S. M., Hurren, N. M., Yfanti, C., Chao, T., Andersen, C. R., Cesani, F., Hawkins, H., and Sidossis, L. S. (2014) Brown adipose tissue improves whole-body glucose homeostasis and insulin sensitivity in humans. *Diabetes* **63**, 4089–4099 [CrossRef Medline](#)
42. Min, S. Y., Kady, J., Nam, M., Rojas-Rodriguez, R., Berkenwald, A., Kim, J. H., Noh, H. L., Kim, J. K., Cooper, M. P., Fitzgibbons, T., Brehm, M. A., and Corvera, S. (2016) Human “brite/beige” adipocytes develop from capillary networks, and their implantation improves metabolic homeostasis in mice. *Nat. Med.* **22**, 312–318 [CrossRef Medline](#)
43. Stanford, K. I., Middelbeek, R. J., Townsend, K. L., An, D., Nygaard, E. B., Hitchcox, K. M., Markan, K. R., Nakano, K., Hirshman, M. F., Tseng, Y. H., and Goodyear, L. J. (2013) Brown adipose tissue regulates glucose homeostasis and insulin sensitivity. *J. Clin. Invest.* **123**, 215–223 [CrossRef Medline](#)
44. Powelka, A. M., Seth, A., Virbasius, J. V., Kiskinis, E., Nicoloso, S. M., Guilherme, A., Tang, X., Straubhaar, J., Cherniack, A. D., Parker, M. G., and Czech, M. P. (2006) Suppression of oxidative metabolism and mitochondrial biogenesis by the transcriptional corepressor RIP140 in mouse adipocytes. *J. Clin. Invest.* **116**, 125–136 [Medline](#)
45. Kiskinis, E., Chatzeli, L., Curry, E., Kaforou, M., Frontini, A., Cinti, S., Montana, G., Parker, M. G., and Christian, M. (2014) RIP140 represses the “brown-in-white” adipocyte program including a futile cycle of triacylglycerol breakdown and synthesis. *Mol. Endocrinol.* **28**, 344–356 [CrossRef Medline](#)
46. Leonardsson, G., Steel, J. H., Christian, M., Pockock, V., Milligan, S., Bell, J., So, P. W., Medina-Gomez, G., Vidal-Puig, A., White, R., and Parker, M. G. (2004) Nuclear receptor corepressor RIP140 regulates fat accumulation. *Proc. Natl. Acad. Sci. U.S.A.* **101**, 8437–8442 [CrossRef Medline](#)
47. Bartz, R., Fan, H., Zhang, J., Innocent, N., Cherrin, C., Beck, S. C., Pei, Y., Momose, A., Jadhav, V., Tellers, D. M., Meng, F., Crocker, L. S., Sepp-Lorenzino, L., and Barnett, S. F. (2011) Effective siRNA delivery and target mRNA degradation using an amphipathic peptide to facilitate pH-dependent endosomal escape. *Biochem. J.* **435**, 475–487 [CrossRef Medline](#)
48. Aouadi, M., Tesz, G. J., Nicoloso, S. M., Wang, M., Chouinard, M., Soto, E., Ostroff, G. R., and Czech, M. P. (2009) Orally delivered siRNA targeting macrophage Map4k4 suppresses systemic inflammation. *Nature* **458**, 1180–1184 [CrossRef Medline](#)
49. Aouadi, M., Tencerova, M., Vangala, P., Yawe, J. C., Nicoloso, S. M., Amano, S. U., Cohen, J. L., and Czech, M. P. (2013) Gene silencing in adipose tissue macrophages regulates whole-body metabolism in obese mice. *Proc. Natl. Acad. Sci. U.S.A.* **110**, 8278–8283 [CrossRef Medline](#)
50. Tesz, G. J., Aouadi, M., Prot, M., Nicoloso, S. M., Boutet, E., Amano, S. U., Goller, A., Wang, M., Guo, C. A., Salomon, W. E., Virbasius, J. V., Baum, R. A., O'Connor, M. J., Jr., Soto, E., Ostroff, G. R., and Czech, M. P. (2011) Glucan particles for selective delivery of siRNA to phagocytic cells in mice. *Biochem. J.* **436**, 351–362 [CrossRef Medline](#)
51. Cohen, J. L., Shen, Y., Aouadi, M., Vangala, P., Tencerova, M., Amano, S. U., Nicoloso, S. M., Yawe, J. C., and Czech, M. P. (2016) Peptide- and amine-modified glucan particles for the delivery of therapeutic siRNA. *Mol. Pharm.* **13**, 964–978 [CrossRef Medline](#)
52. Kim, S., Kim, D., Cho, S. W., Kim, J., and Kim, J. S. (2014) Highly efficient RNA-guided genome editing in human cells via delivery of purified Cas9 ribonucleoproteins. *Genome Res.* **24**, 1012–1019 [CrossRef Medline](#)
53. Zischewski, J., Fischer, R., and Bortesi, L. (2017) Detection of on-target and off-target mutations generated by CRISPR/Cas9 and other sequence-specific nucleases. *Biotechnol. Adv.* **35**, 95–104 [CrossRef Medline](#)
54. Schaefer, B. C., Schaefer, M. L., Kappler, J. W., Marrack, P., and Kedd, R. M. (2001) Observation of antigen-dependent CD8⁺ T-cell/ dendritic cell interactions *in vivo*. *Cell Immunol.* **214**, 110–122 [CrossRef Medline](#)
55. Scheller, J., Chalaris, A., Schmidt-Arras, D., and Rose-John, S. (2011) The pro- and anti-inflammatory properties of the cytokine interleukin-6. *Biochim. Biophys. Acta* **1813**, 878–888 [CrossRef Medline](#)
56. Pedersen, B. K., Steensberg, A., and Schjerling, P. (2001) Muscle-derived interleukin-6: possible biological effects. *J. Physiol.* **536**, 329–337 [CrossRef Medline](#)
57. Christian, M., Kiskinis, E., Debevec, D., Leonardsson, G., White, R., and Parker, M. G. (2005) RIP140-targeted repression of gene expression in adipocytes. *Mol. Cell Biol.* **25**, 9383–9391 [CrossRef Medline](#)
58. Arner, P., Bernard, S., Salehpour, M., Possnert, G., Liebl, J., Steier, P., Buchholz, B. A., Eriksson, M., Arner, E., Hauner, H., Skurk, T., Rydén, M., Frayn, K. N., and Spalding, K. L. (2011) Dynamics of human adipose lipid turnover in health and metabolic disease. *Nature* **478**, 110–113 [CrossRef Medline](#)
59. Doench, J. G., Fusi, N., Sullender, M., Hegde, M., Vaimberg, E. W., Donovan, K. F., Smith, I., Tothova, Z., Wilen, C., Orchard, R., Virgin, H. W., Listgarten, J., and Root, D. E. (2016) Optimized sgRNA design to maximize activity and minimize off-target effects of CRISPR-Cas9. *Nat. Biotechnol.* **34**, 184–191 [CrossRef Medline](#)
60. Labun, K., Montague, T. G., Gagnon, J. A., Thyme, S. B., and Valen, E. (2016) CHOPCHOP v2: a web tool for the next generation of CRISPR genome engineering. *Nucleic Acids Res.* **44**, W272–W276 [CrossRef Medline](#)
61. Montague, T. G., Cruz, J. M., Gagnon, J. A., Church, G. M., and Valen, E. (2014) CHOPCHOP: a CRISPR/Cas9 and TALEN web tool for genome editing. *Nucleic Acids Res.* **42**, W401–W407 [CrossRef Medline](#)
62. Wang, X., Tilford, C., Neuhaus, I., Mintier, G., Guo, Q., Feder, J. N., and Kirov, S. (2017) CRISPR-DAV: CRISPR NGS data analysis and visualization pipeline. *Bioinformatics* **33**, 3811–3812 [CrossRef Medline](#)